



2 Stress field evolution in the northwest Himalayan syntaxis, 3 northern Pakistan

4 A. Pêcher,¹ L. Seeber,² S. Guillot,¹ F. Jouanne,³ A. Kausar,⁴ M. Latif,⁴ A. Majid,⁴
5 G. Mahéo,⁵ J. L. Mugnier,³ Y. Rolland,⁶ P. van der Beek,¹ and J. Van Melle¹

6 Received 21 December 2007; revised 17 July 2008; accepted 11 September 2008; published XX Month 2008.

8 [1] We have conducted a systematic inversion of
9 striated fault planes throughout northern Pakistan in
10 order to better depict the temporal and spatial
11 variations in stress patterns. Two domains are
12 evidenced at a regional scale, separated by the active
13 Raikhot fault, the western boundary of the Nanga
14 Parbat spur. West of this fault, a wrench-type stress
15 field with σ_1 axis oriented around N–S predominates
16 in the Karakorum and in Kohistan. It predates
17 Pliocene-Quaternary exhumation of Nanga Parbat
18 and corresponds to the Miocene or earlier regional
19 stress field related to Indian-Asian convergence. East
20 of the Raikhot fault, compression parallel to the belt
21 accounts for initiation of the Nanga Parbat
22 anticlinorium after 5 Ma. It is followed by
23 predominant post-2 Ma extension, both parallel to
24 the belt and NNE–SSW oriented. Thus, in the N–W
25 Himalayan syntaxis, multidirectional extension is
26 juxtaposed on short timescales to shortening either
27 parallel or perpendicular to the belt. Such juxtaposition
28 could be characteristic of strain and stress partitioning
29 during oblique convergence. **Citation:** Pêcher, A., et al.
30 (2008), Stress field evolution in the northwest Himalayan
31 syntaxis, northern Pakistan, *Tectonics*, 27, XXXXXX,
32 doi:10.1029/2007TC002252.

34 1. Introduction

35 [2] The Himalayan syntaxes have attracted significant
36 attention in recent years because they provide strong indi-
37 cations for coupling between tectonic and surface processes
38 responsible for extremely rapid exhumation documented in
39 the Nanga Parbat (in the NW syntaxis) and Namche Barwa
40 (SE syntaxis) massifs, respectively [e.g., Zeitler *et al.*,

2001a, 2001b; Burg *et al.*, 1998]. Less attention has been
41 paid, however, to the tectonic evolution of these regions,
42 and in particular how stress and strain fields evolved to
43 produce the highly complex, noncylindrical structural pat-
44 terns observed today. In particular, if tectonics and surface
45 processes strongly interact in these regions, we may ask the
46 question whether (and if so, how) this interaction is
47 recorded by the evolving regional stress fields. 48

[3] Neotectonic activity in the NW Himalaya has been
49 dramatically emphasized by the recent $M = 7.6$ Balakot
50 earthquake in Kashmir (8 October 2005). The Balakot
51 earthquake followed the Pattan 1974 earthquake, the epi-
52 center of which was located 100 km farther NW. The focal
53 mechanisms of both earthquakes reveal active thrusting in a
54 NE–SW shortening regime, perpendicular to the average
55 orientation of northwestern Himalaya. A few tens of km
56 farther north, in contrast, a recent microseismicity survey
57 has revealed an active E–W extensional regime in the
58 Nanga Parbat area, while the adjacent Kohistan block
59 appears to be nearly aseismic [Meltzer *et al.*, 2001]. Such
60 a juxtaposition of different tectonic regimes underlines the
61 complex stress and strain pattern in this part of Himalaya: the
62 northwestern Himalaya-Karakorum belt is a typical case of a
63 mountain chain formed by transpressional tectonics, in which
64 strain partitioning has probably controlled the Pliocene-
65 Quaternary tectonics [Seeber and Pêcher, 1998], and where
66 exhumation patterns and its driving forces have varied
67 temporally and spatially [Zeitler, 1985]. 68

[4] In order to better depict the temporal and spatial
69 variations in stress patterns, we have conducted a systematic
70 inversion of striated faults planes observed in outcrops
71 throughout the northern Pakistan Himalaya. We collected
72 data in a broad area of northern Pakistan, from the Hunza,
73 Gilgit and Indus valleys in the west, to Deosai and Skardu
74 area in the east, and Jhelum valley in the south (Figure 1).
75 Our results complete a preliminary study in the same area
76 [Pêcher and Seeber, 2003] and broaden the local inves-
77 tigation of Zeilinger *et al.* [2000] in the southern part of the
78 Kohistan arc along the Indus valley and Burg *et al.* [2005b]
79 in the Kashmir syntaxis. 80

[5] As compared to similar but older mountain belts, the
81 NW Himalaya seems particularly propitious to such an
82 analysis: to a large extent, inferred paleostress tensors
83 should reflect the recent stress field, as in several areas
84 (i.e., Karakorum, Nanga Parbat, Kashmir) brittle deforma-
85 tion is superimposed on a ductile deformation pattern
86 acquired during early Pliocene times, or possibly even later.
87 In these areas, the paleostress pattern should be similar to
88 the current stress field, which allows some direct control of
89

¹Laboratoire de Géodynamique des Chaînes Alpines, CNRS, Université de Grenoble, Grenoble, France.

²Lamont-Doherty Earth Observatory, Earth Institute at Columbia University, Palisades, New York, USA.

³Laboratoire de Géodynamique des Chaînes Alpines, CNRS, Université de Savoie, Le Bourget du Lac, France.

⁴Geological Survey of Pakistan, Islamabad, Pakistan.

⁵Laboratoire de Sciences de la Terre, CNRS, Université de Lyon 1 et École Normale Supérieure de Lyon, Villeurbanne, France.

⁶Géosciences Azur, UMR 6526, CNRS, Université de Nice, Nice, France.

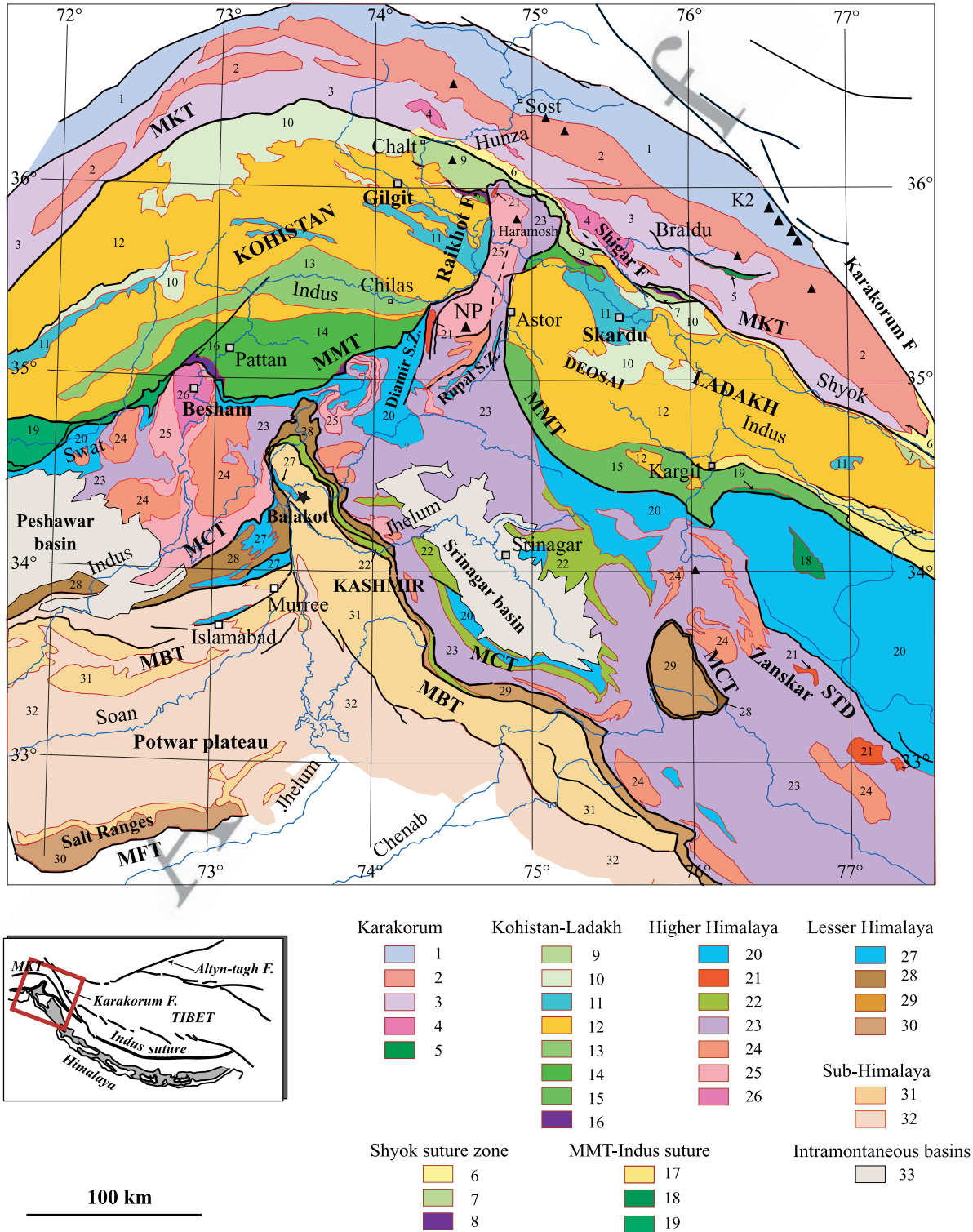


Figure 1

90 the results, and could give a picture of the stress field
91 responsible for the present-day seismicity. In contrast, zones
92 that have apparently been stable since a long period (e.g.,
93 Deosai or Kohistan) could have kept traces of older (pre-
94 Pliocene) stress patterns.

95 2. Tectonic and Morphologic Framework of 96 Northern Pakistan

97 [6] At a broad scale, the Himalayan mountain belt can be
98 divided into two segments separated by the Karakorum
99 fault, a 1000-km-long right-lateral shear zone, active at
100 least since 21 Ma until 4 Ma [Valli *et al.*, 2007]. Slip rate
101 estimate averaged on the Pleistocene to present time period
102 is 15 to 30 mm a⁻¹ [Armijo *et al.*, 1989; Avouac and
103 Tapponnier, 1993]. East of this fault, the WNW–ESE to
104 W–E strike of the central and eastern Himalaya is nearly
105 perpendicular to the mean orientation of continent-continent
106 convergence [e.g., Bendick and Bilham, 2001; Paul *et al.*,
107 2001]. Shortening is absorbed mainly by large thrusts and
108 folds striking parallel to the belt, and structures are pre-
109 dominantly cylindrical. West of the Karakorum fault, in
110 contrast, the NW Himalaya (including most of Indian
111 Ladakh and northern Pakistan) has an average NW–SE
112 strike, oblique to Indian-Asian convergence. This obliquity
113 induces a complex strain pattern, in which shortening
114 orientations perpendicular and parallel to the belt are
115 juxtaposed or superimposed, while a large amount of
116 displacement is absorbed along strike-slip shear zones.

117 [7] A central element of the NW Himalaya is the Kohi-
118 stan-Ladakh Arc complex, which separates Indian and
119 Asian plate rocks (Figure 1). The Kohistan-Ladakh arc
120 collided with the Asian margin prior to 75 Ma, and was
121 later partly obducted onto the Indian margin [Coward *et al.*,
122 1987]. It now forms a piece of arc crust, characterized by

basic-intermediate rocks, pinched between the Karakorum 123
and Himalayan continental crusts. The Karakorum series 124
have been thrust onto the Cretaceous-Tertiary back-arc 125
formations of the Shyok suture zone [Sharma and Gupta, 126
1978; Robertson and Collins, 2002] along the Main 127
Karakorum Thrust (MKT) Along the MKT, north-south 128
shortening structures, prior to 40 Ma, are overprinted by 129
poorly dated dextral strike-slip displacement, combined to 130
SE directed overthrusting [Coward *et al.*, 1986]. In its turn, 131
the Kohistan-Ladakh arc has been thrust southward over the 132
Indian crust along the Main Mantle Thrust (MMT) 133
[Tahirikheli *et al.*, 1979; Tahirikheli, 1982], and the Indian 134
crust has been thickened by thrusting along the Miocene 135
Main Central Thrust (MCT), the post-Miocene Main 136
Boundary Thrust (MBT) and the currently active Main 137
Frontal Thrust (MFT). 138

[8] The most complete tectonic and metamorphic evolu- 139
tion of the NW Himalaya is recorded within the Karakorum 140
series (i.e., north of the MKT, on the Asian side of the belt). 141
Here metamorphism started early, probably before 64 Ma, 142
followed by a distinct event around 44 Ma [Searle *et al.*, 143
1999; Fraser *et al.*, 2001]. The main metamorphic phase 144
M1 [Rolland *et al.*, 2001, 2006] ended before emplacement 145
of the Baltoro granite at 21 Ma [Parrish and Tirrul, 1989], 146
but thrust-driven stacking of the units was active up to 147
16 Ma, as dated by metamorphic monazites in the Hunza 148
valley [Fraser *et al.*, 2001], and possibly up to 9 Ma, as 149
indicated by Ar-Ar ages of muscovite in thrust-related 150
schistosity in the Chogo Lungma area [Villa *et al.*, 1996]. 151
Same age crustal melting at depth is attested by the Sumayar 152
leucogranite dated at 9.2 Ma [Fraser *et al.*, 1999]. Fission 153
track [Poupeau *et al.*, 1991] and Ar/Ar [Krol *et al.*, 1996] 154
age profiles east of the Hunza valley in the central Kar- 155
akorum reveal rapid exhumation (~3 mm a⁻¹) between 20 156
and 12 Ma, followed by much slower rates (0.7 mm a⁻¹) 157

Figure 1. Geological map of the NW Himalaya. Main tectonic boundaries: MKT, Main Karakorum Thrust; MMT, Main Mantle Thrust (Indus Suture Zone); STD, South Tibetan Detachment; MCT, Main Central Thrust; MBT, Main Boundary Thrust; MFT, Main Frontal Thrust. Geological units, from north to south: Unit A Karakorum: 1, northern sedimentary belt; 2, axial batholith and other granitoids; 3, southern metamorphic belt; 4, felsic gneiss; 5, greenstone complex, Paleozoic (Masherbrum complex). Unit B Shyok suture zone: reactivated along the MKT, 6, predominantly terrigenous formation; 7, melange zone, predominantly volcanics; 8, ultramafics (Shyok and Dobani-Dassu lineament). Unit C Kohistan: 9, Eocene Chalt (Kohistan) and Kardung (Ladakh) volcanics, Turmik volcanosediments; 10, undifferentiated volcanosedimentary group; 11, metasediments; 12, plutonic rocks (Kohistan and Ladakh batholith); 13, gabbro-norites (Chilas complex); 14, southern amphibolites (Kohistan); 15, Dras volcanosedimentary group (Ladakh); 16, mantle ultrabasites (Jijal complex). Unit D MMT-Indus suture zone: 17, Indus molasses; 18, Spontang ophiolites; 19, imbricate thrust units, with blue schists. Unit E Higher Himalaya: 20, Neotethyan sedimentary group (Permian-Eocene); 21, Tertiary leucogranites (Ladakh and Nanga Parbat); 22, Panjal Traps (Permian); 23, High Himalaya Crystalline (mainly metasediments, Late Proterozoic to early Paleozoic); 24, Paleozoic intrusives (Swat and Manserah granite, Kohistan, Bhazum and Kade granite, Ladakh); 25, basement gneiss (dominantly Early Proterozoic orthogneiss); 26, Besham metagneous. Unit F Lesser Himalaya: 27, Paleozoic-Eocene cover; 28, upper nappe, dominantly Early Proterozoic metasediments (Abbottabad, Kishtwar); 29, lower nappe, dominantly Late Proterozoic–Paleozoic metasediments (Kishtwar, Kashmir); 30, Salt Ranges (Late Proterozoic–Eocene Indian cover). Unit G Sub-Himalaya: 31, Muree and Subatu formations (Eocene to Miocene); 32, Siwaliks (middle Miocene to Quaternary); 33, Peshawar and Srinagar intramontaneous basins (Quaternary). Personal data and modified from Bossart and Ottiger [1989], Burbank *et al.* [1986], Greco *et al.* [1989], Burg *et al.* [2005a], DiPietro *et al.* [2000], DiPietro and Pogue [2004], Edwards *et al.* [2000], Fontan *et al.* [2000], Gaetani [1997], Greco [1991], Kasmir and Jan [1997], Le Fort and Pêcher [2002], Lombardo and Rolfo [2000], Reuber [1989], Rolland *et al.* [2000, 2002], Schneider *et al.* [2001], Steck [2003], Tahirikheli [1996], Valdiya [1998], Wadia [1975], and Zanchi and Gaetani [1994].

158 from 6.6 to 2.4 Ma. Strong Mio-Pliocene and Quaternary
 159 tectonic reactivation, accompanied by rapid exhumation of
 160 middle and lower crustal rocks, led to the present-day relief
 161 of Karakorum, characterized by high summits with altitudes
 162 reaching >7500 m, strong incision of rivers that cut down to
 163 altitudes <2000 m, and steep slopes. Tectonics appears
 164 mainly active in the eastern Karakorum, where the highest
 165 peaks of the NW Himalaya occur (with five peaks over
 166 8000m, among which K2, 8611 m). Here, Neogene tecton-
 167 ism is manifested by a series of dome-shaped anticlines
 168 aligned along the east–west Braldu line [Bertrand *et al.*,
 169 1988; Rolland *et al.*, 2001]. In the domes, most low- and
 170 intermediate-temperature thermochronological systems re-
 171 cord Plio-Pleistocene cooling ages, revealing recent rapid
 172 exhumation from midcrustal depths. The domes initially
 173 grew as transpressional folds, initiated in a tectonic corridor
 174 bounded by two NW–SE faults [Pêcher and Le Fort, 1999;
 175 Rolland *et al.*, 2001; Mahéo *et al.*, 2004]: the major and
 176 currently active Karakorum fault to the NE, along which the
 177 highest peaks are lined up, and the parallel Shigar fault to
 178 the SW (Figure 1). The latter fault should have a recent
 179 vertical offset of more than 2 km, but we have not been able
 180 to find any indication of late Quaternary activity in the field.
 181 The domes evolved by rapid diapiric amplification within
 182 migmatized anticline cores, with exhumation rates attaining
 183 5.5 mm a^{-1} from 6.7 to 4.7 Ma (Ar–Ar cooling ages ranging
 184 up to 4.7 Ma [Searle *et al.*, 1989]), and were finally exposed
 185 during E–W buckling and uplift of the whole southeast
 186 Karakorum [Mahéo *et al.*, 2004].

187 [9] South of the MKT, the Kohistan Arc formations crop
 188 out in two broad blocs on each side of the Nanga Parbat
 189 spur, Kohistan to the west and Ladakh to the east, linked
 190 north of the Nanga Parbat by a thin strip of arc volcanites
 191 and metasediments. Kohistan and Ladakh have been free of
 192 Miocene or younger reactivation. They have a similar
 193 average elevation as adjacent high-relief areas of Karako-
 194 rum and Nanga Parbat, but with a much smoother relief.
 195 The most striking example of such high-elevation, low-
 196 relief areas is the Deosai plateau in Pakistani Ladakh, a
 197 conspicuously flat plateau at around 4000 m elevation
 198 between the Nanga Parbat massif to the west, the Indus
 199 valley to the north and the Shigar valley to the east.
 200 Recently acquired low-temperature thermochronology data
 201 from the Deosai plateau indicate slow exhumation between
 202 40 and 20 Ma, bracketed by zircon (U–Th)/He, and apatite
 203 FT and (U–Th)/He ages [Van Melle *et al.*, 2007]. The
 204 recorded slow and continuous exhumation implies that the
 205 plateau probably attained its modern morphology already
 206 long before 20 Ma.

207 [10] Between Kohistan and Ladakh, the Nanga Parbat–
 208 Haramosh spur corresponds to a crustal-scale, N–S elon-
 209 gated dome [Schneider *et al.*, 2001] exhuming a window of
 210 Himalayan gneisses from below the Kohistan arc rocks of
 211 the MMT hanging wall. In the Nanga Parbat area, the MMT
 212 has been refolded into a broad N–S anticline. Because of
 213 this fold, ductile mylonites related to the MMT crop out on
 214 both sides of the Nanga Parbat spur in two shear zones, with
 215 apparent right-lateral (eastern side) and left-lateral (western
 216 side) movements, respectively [Edwards *et al.*, 2000]. In the

Nanga Parbat gneisses, Ar–Ar cooling ages on biotite range 217
 from 5 Ma in the limbs of the fold to 1 Ma in its core 218
 [Schneider *et al.*, 2001], with intrusive leucogranite lenses 219
 as young as 1.4 Ma [Zeitler *et al.*, 1993]. West of the fold, 220
 the Raikhot fault reactivates the MMT and Diamir shear 221
 zone. Along this fault, the western limb of the Nanga Parbat 222
 overthrusts Pleistocene Indus alluvial terraces [Butler and 223
 Prior, 1988]. Together with the strong relief [Burbank *et al.*, 224
 1996], similar to the Karakorum, the distribution of the 225
 Pliocene–Quaternary cooling ages, and the earthquake focal 226
 mechanisms (Figure 2), evidence the fast amplification of 227
 the fold from upper Miocene up to present, as a pop-up 228
 anticline [Edwards *et al.*, 2000] exhuming in a regime of 229
 east–west shortening. 230

[11] Southwest of Nanga Parbat, the Besham syntaxis 231
 (Figure 1) also corresponds to a N–S trending anticline. It 232
 indicates a similar origin as for Nanga Parbat but at a less 233
 evolved stage. In this area, Zeilinger *et al.* [2000] have 234
 proposed a complex tectonic history, inferring from the 235
 inversion of fault data the probable superposition of three 236
 different stress fields since late Miocene times. 237

[12] South of Nanga Parbat, the southern Himalayan 238
 accretionary prism constitutes a fold-and-thrust belt involv- 239
 ing the MCT, the MBT and the MFT. It is a region of 240
 intermediate relief, juxtaposing flat basins such as the 241
 Peshawar and Shrinagar basins and the Potwar Plateau 242
 (Figure 1) with zones marked by active erosion, deep 243
 valleys, steep sidewalls, but no high summits. The tectonic 244
 pattern is complex, mimicking the one observed farther 245
 north in Nanga Parbat. After southward thrusting of the 246
 Lesser Himalayan formations onto Miocene series along the 247
 MBT, the entire pile was refolded in a north–south trending 248
 anticline, which provides evidence for E–W shortening. 249
 Earthquake focal mechanisms, in contrast, indicate active 250
 NE–SW shortening, perpendicular to the regional trend of 251
 the NW Himalaya (Figure 2). 252

[13] In summary, the northwest Himalayan syntaxis dis- 253
 plays a present-day geological pattern made of a puzzle of 254
 clearly identifiable large blocks, with contrasting evolu- 255
 tions. Some areas are apparently passive since Miocene, 256
 while some others reveal active Pliocene–Quaternary ductile 257
 tectonics. The timing of brittle deformation should thus be 258
 different from one block to another. In the zone of recent 259
 exhumation (Karakorum dome, Nanga Parbat), it can be 260
 roughly bracketed using Ar/Ar cooling ages: the closure 261
 temperature for biotite is commonly quoted as $300 \pm 50^\circ\text{C}$ 262
 [e.g., Harrison *et al.*, 1985; MacDougall and Harrison, 263
 1999], although it might be significantly higher depending 264
 on chemical composition [Grove and Harrison, 1996]. This 265
 temperature is 150° lower than the currently accepted 266
 temperature for the ductile–brittle transition in the crust 267
 ($300\text{--}450^\circ\text{C}$) [Scholz, 1988, 2002; Viganò and Martin, 268
 2007], thus the change from ductile to brittle deformation 269
 should be slightly older than the biotite ages. Nevertheless, 270
 in areas of rapid cooling and exhumation, this time discrep- 271
 ancancy will be small (typically ≤ 1 Ma). Accordingly, brittle 272
 deformation in the Karakorum domes or the Nanga Parbat 273
 anticline should be mainly late Pliocene or Quaternary in 274
 age. In contrast, in Kohistan and Ladakh (particularly on the 275

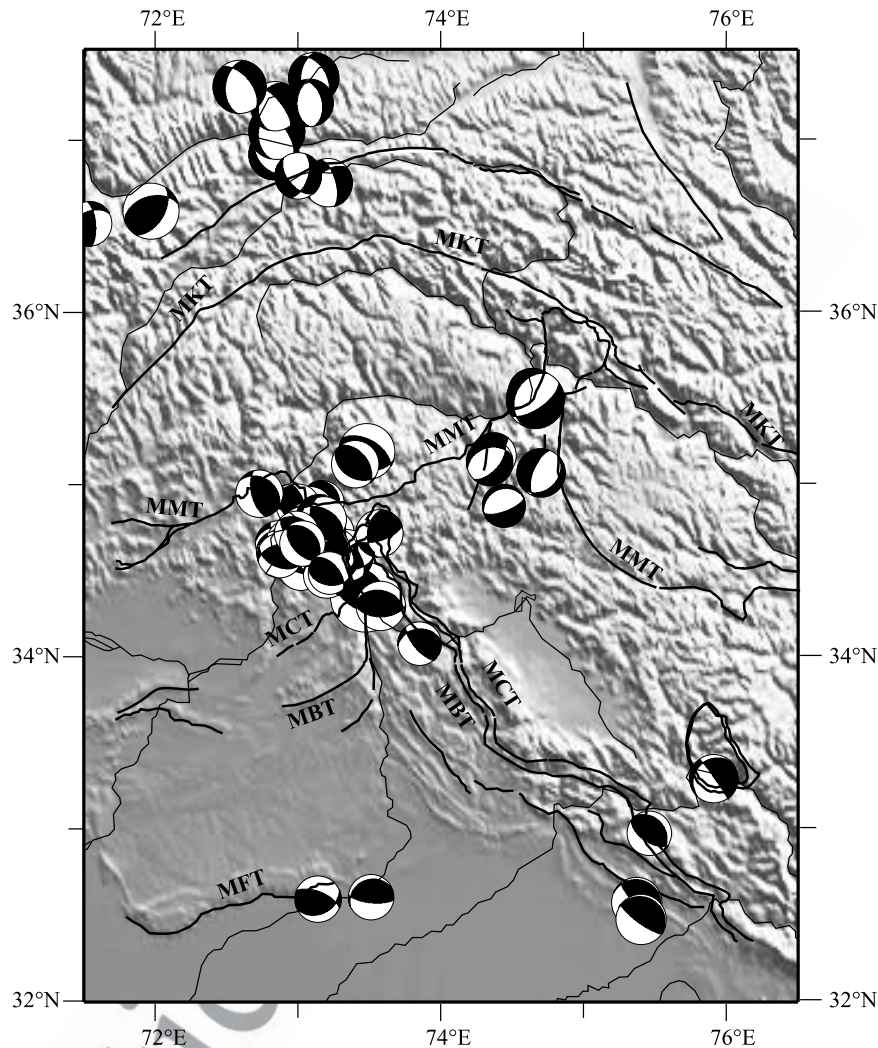


Figure 2. Focal mechanism solutions in NW Himalaya, CMT solutions. White indicates P axis quadrant, black indicates T axis quadrant. See Global CMT Web page <http://www.globalcmt.org/>.

276 Deosai Plateau, already cooled 20 Ma ago), one can expect
 277 the fault data to retain a memory of the stress state prior to
 278 Miocene-Quaternary exhumation of Nanga Parbat and Kar-
 279 akorum, even if older brittle faults in those areas could have
 280 been reactivated during these late events. In the Siwaliks
 281 formations, the main deformation phase is post-Miocene, as
 282 evidenced by the folding of the Tertiary Siwalik series,
 283 together with the MCT and the MBT, in sharp N–S trending
 284 folds in the Kashmir syntaxis. The timing of the brittle
 285 deformation is currently poorly constrained. *Burg et al.*
 286 [2005b] provide evidence from fault analysis for two
 287 successive paleostress orientations, with predominant NE–
 288 SW and E–W compression, respectively. Their relative
 289 chronology remains unknown. Nevertheless, we note that
 290 E–W compression is coherent with the east–west shorten-
 291 ing evidenced by the folding of Miocene series and MBT in
 292 the Hazara Kashmir syntaxis, while NW–SE compression

fits with the focal mechanisms and displacements deduced
 from earthquakes (Figure 2).

3. Methodology

[14] Several methods have been developed to use sets of
 fault planes and slickenlines with kinematic indicators to
 depict paleostress tensors. Most of them are based on the
 concept of the reduced stress tensor; that is, they aim to
 determine the orientation of the principal stress axes σ_1 , σ_2 ,
 σ_3 (with $\sigma_1 \geq \sigma_2 \geq \sigma_3$ and compression being positive)
 together with a shape parameter. The shape parameter can
 be either *Lode's* [1925] parameter $\mu = (2\sigma_2 - \sigma_1 - \sigma_3)/(\sigma_1$
 $- \sigma_3)$, *Bishop's* [1966] parameter $\Phi = (\sigma_2 - \sigma_3)/(\sigma_1 - \sigma_3)$
 [e.g., *Angelier*, 1975, 1979, 1984; *Yamaji*, 2000], or the
 similar parameter $R_0 = (\sigma_1 - \sigma_2)/(\sigma_1 - \sigma_3)$ [e.g., *Célérier*,
 1995; *Zeilinger et al.*, 2000; *Burg et al.*, 2005b]. All
 inversion methods rely on several assumptions: (1) the

309 stress is uniform over the volume where the fault data for
 310 the inversion are measured; (2) the stress tensor is equiva-
 311 lent to the incremental deformation tensor, as obtained from
 312 the slip data; and (3) the basic hypothesis of *Bott* [1959],
 313 which considers that the slip vector on a plane, as given by
 314 the slickenlines in the case of striated fault planes, is parallel
 315 to the maximum shear stress along the fault plane as
 316 deduced from the stress tensor. Because of the nonideal
 317 conditions (for instance, guided movement of the various
 318 blocks cut by the faults, non infinitesimal displacements,
 319 etc.), some discrepancy is accepted. The quality of the
 320 inversion is estimated from the angular misfits between
 321 theoretical striae predicted from the calculated tensor and
 322 the measured striae.

323 [15] In the case of an area where the amount of deforma-
 324 tion is small and all fault movements observed at a given
 325 scale (typically on an outcrop of a few tens of square
 326 meters) result from a uniform stress field, direct inversion
 327 by purely analytical means (i.e., a search of the tensor which
 328 minimizes angular misfits, as proposed, for instance, by
 329 *Angelier* [1975]) yields similar stress parameters regardless
 330 of the methods. In such cases, a good preliminary estimate
 331 of the orientation of the stress axes can in fact usually
 332 already be given in the field from observations of conjugate
 333 fault sets, and the numerical stress inversion mainly adds the
 334 shape parameter of the stress ellipsoid.

335 [16] In most natural cases, however, the observed brittle
 336 structures record a complex tectonic history, with superpo-
 337 sition of several stress states in the same area. When dealing
 338 with the resulting heterogeneous fault slip data (i.e., where
 339 not all faults slipped in response to the same deviatoric
 340 stress, and where newly formed faults are combined with
 341 reactivated fractures), separation of stress tensors becomes a
 342 challenging target. The problem has been addressed in
 343 several ways. It is possible to separate subsets of faults
 344 from the data set, based on geological considerations: for
 345 instance, evidence of reactivation of faults, with crosscut-
 346 ting relationships or superimposition of striae; separation of
 347 fault sets based on differences in mineral coatings; or in case
 348 of an assumed Andersonian geometry (one of the principal
 349 stress orientations approximately vertical and the other two
 350 horizontal), a priori separation of normal and transtensional
 351 faults (corresponding to horizontal extension) from reverse
 352 or transpressional faults (horizontal shortening). Alterna-
 353 tively, semiautomatic or automatic approaches attempt to
 354 extract the set of tensors that best fits the given set of faults,
 355 independent of geological criteria. In semiautomatic meth-
 356 ods, a first tensor is computed, which minimizes the sum of
 357 the angular misfits. The method is then applied recursively
 358 to subsets of the data that show large misfits from slip
 359 directions predicted from formerly determined stress tensors
 360 [e.g., *Etchecopar et al.*, 1981; *Armijo et al.*, 1982]. Auto-
 361 matic determination of the tensor can also be based on
 362 statistical techniques of cluster analysis (see *Nemcok and*
 363 *Lisle* [1995], who group the faults in dynamic subsets prior
 364 to normal stress inversion). In multiple inverse methods
 365 [*Yamaji*, 2000; *Otsubo et al.*, 2006], significant solutions
 366 calculated on small subsets of faults are identified as
 367 clusters in the parameters space. Whatever the method,

however, it appears that inversion of heterogeneous fault 368
 slip data cannot be fully automated and implies “researcher 369
 decisions” [*Liesa and Lisle*, 2004]. 370

3.1. Measuring the Data 371

[17] Altogether, we have measured more than 2800 fault/ 372
 striation pairs from 120 sites (Figure 3 and Table S1 in the 373
 auxiliary material)¹, spread from the Salt Ranges to the 374
 northern Karakorum. Each site corresponds to between 375
 8 and 43 measurements (generally around 25) on a single 376
 outcrop or on a section no longer than 50 m. The quality of 377
 measurement was noted (in particular the degree of confi- 378
 dence in the inferred sense of movement); where the quality 379
 was weak (usually because of an unclear sense of move- 380
 ment), the fault was either rejected or labeled as suspect. 381
 The presence and nature of crystallization on the fault plane 382
 was noted in order to attempt to separate sets of different 383
 ages, but no clear general distinction has resulted from this 384
 sorting. 385

[18] Most of our measurement sites are along fresh road 386
 cuts. On such sections, an exhaustive view of all faults is 387
 easy to obtain, while it is often difficult to find sufficient 388
 faults and good quality movement criteria in natural out- 389
 crops. Accordingly, our network of stations is irregularly 390
 spaced: it is dense in the Nanga Parbat–Haramosh area, 391
 which is traversed by the Karakorum Highway, the Skardu 392
 road and the Astor-Deosai road, but sparser within the 393
 Karakorum Range and nearly empty in the southern part 394
 of Nanga Parbat, which is a restricted area close to the 395
 India-Pakistan Line of Control. Only a few sites have been 396
 measured along the Karakorum Highway in the Pattan area, 397
 where the MMT forms a north–south trending fold suggest- 398
 ing a growing (or aborted) structure similar to Nanga Parbat. 399
 This section has been studied in detail by *Zeilinger et al.* 400
 [2000]. Farther south, in the southern Himalayan fold-and- 401
 thrust belt (Hazar-Kashmir syntaxis and frontal Salt 402
 Ranges), propitious outcrops are scarce. We have measured 403
 only about 10 sites, which augment the data obtained by 404
Burg et al. [2005b]. Thus we can compare results obtained 405
 using different inversion methods (inversion with the FSA 406
 software of *Célérier* [1995] for the previous authors, mul- 407
 tiple inverse method of *Yamaji* [2000] for this study). 408

3.2. Processing the Data 409

[19] In most of the measurements sites, faults orientations 410
 are dispersed, and faults cannot be easily grouped in subsets 411
 based on geological criteria. There are numerous indications 412
 for superimposition of movements, but relative chronology 413
 criteria are rare and often ambiguous (for instance, several 414
 tests on planes with superposed striae show that the relative 415
 chronology is subject to observer bias). Therefore, in most 416
 cases the separation of fault subsets in the field prior to their 417
 numerical treatment was at best unclear, and the determi- 418
 nation of the relative chronology of the tensors based on 419
 local geological criteria mostly unsuccessful. 420

¹Auxiliary materials are available in the HTML. doi:10.1029/2007TC002252.

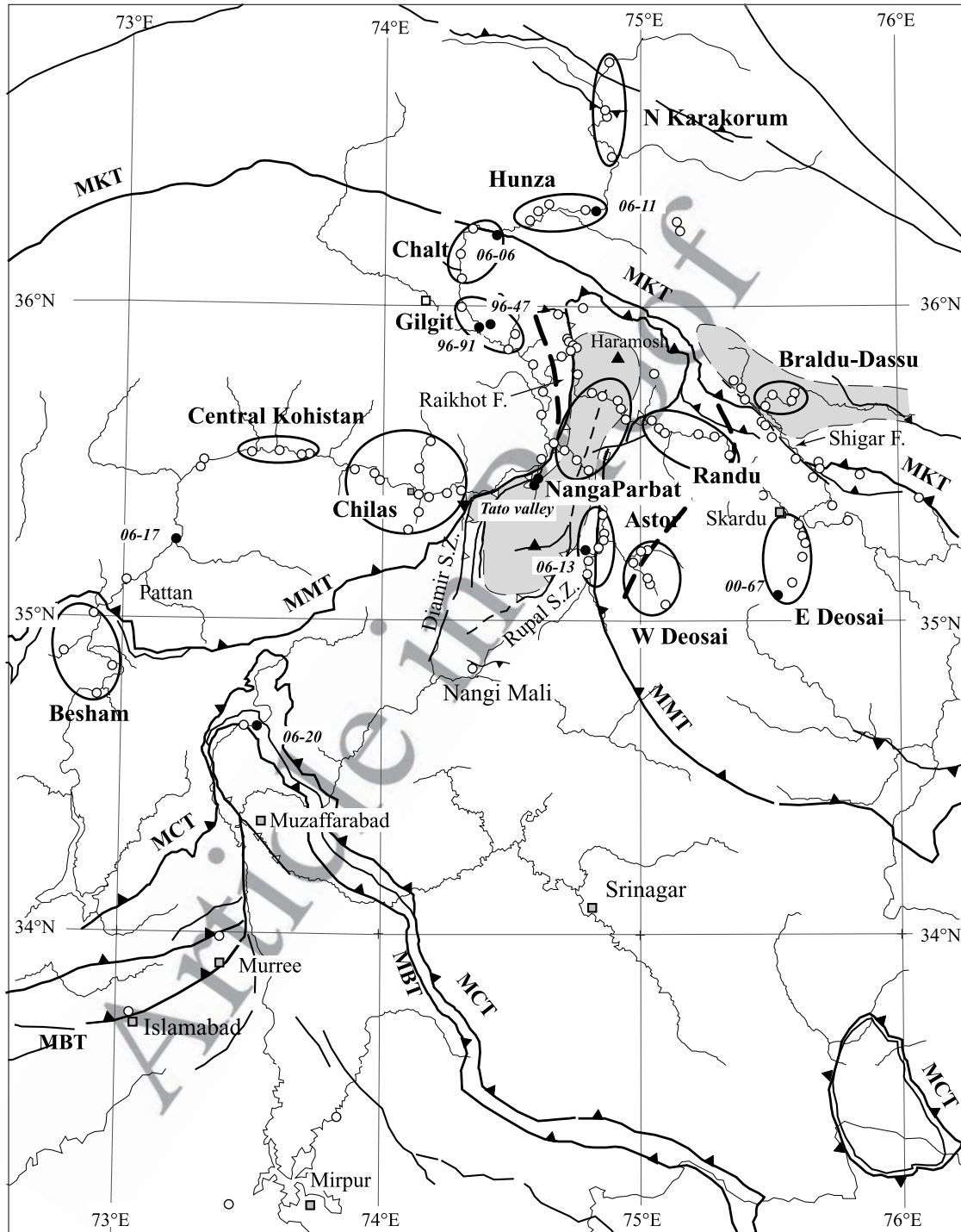


Figure 3. Localization of the fault stations (plain dots) and identification of the grouped sites. Black symbols and reference numbers indicate sites referred to in the text (see Figures 6 and 9). Shaded area indicates zones of Plio-Quaternary very active exhumation (core of the Nanga Parbat pop-up anticline, SE Karakorum domes). Thick dotted line indicates Nanga Parbat morphological limit.

421 [20] Accordingly, we have favored a mainly automatic
 422 approach for treating our data. We used the multiple
 423 inverse method, as developed in the software package
 424 mim5-miv4 of A. Yamaji et al. (Multiple Inverse Method
 425 Software Package, Freeware package, 2005, [http://](http://www.kueps.kyoto-u.ac.jp/~yamaji/PDS/indexe.html)

www.kueps.kyoto-u.ac.jp/~yamaji/PDS/indexe.html). The
 426 method is based on the direct determination of stress
 427 tensors on all small subsets of faults (typically 4 to 6
 428 faults) that can be extracted from the given larger set of
 429 measurements collected in a station. The method uses a
 430

431 computational grid of 60 000 points, the optimal stress
 432 being approximated by the nearest grid point. Points of
 433 the grid with a significant number of solutions tied to it
 434 are plot in a stereogram. Significant stresses will be
 435 revealed on the stereogram by clusters of solutions
 436 sharing a similar shape ratio. According to *Liesa and*
 437 *Lisle* [2004], this method achieves good solutions under
 438 general conditions, provided that the number of faults in
 439 the different subgroups leading to the determination of
 440 the different tensors is similar; minor stress tensors are
 441 difficult to detect.

442 [21] To process the data, we followed a multistep ap-
 443 proach, similar to that of *Zeilinger et al.* [2000]: in areas
 444 where our network of sites was sufficiently dense, we have
 445 attempted to average the regional stress field at a scale of a
 446 few tens of kilometers by grouping the sites located in a
 447 geologically and tectonically homogeneous unit, and pro-
 448 cessing them as a single site (Figure 3). In the case of a
 449 heterogeneous stress field (due to superposition of several
 450 tensors), the large number of faults considered allows a
 451 more robust determination of the tensors, each tensor being
 452 calculated on a large subset of faults. To illustrate our
 453 approach, we will treat the example of the Gilgit area in
 454 some detail below. Data from each station were subsequently
 455 individually processed.

456 [22] Finally, for interpretation and discussion of the
 457 results we define “tilted” and “untilted” tensors. Whatever
 458 the tectonic regime (compression, wrench or extension), it is
 459 generally assumed, following Andersonian fault theory, that
 460 one of the principal stress orientations is approximately
 461 vertical and the other two horizontal [*Célérier, 1995*]. In
 462 fact, we often obtain both “untilted” tensors (tensors for
 463 which one main axis is close to vertical and the other two
 464 close to horizontal) and “tilted” tensors (for which none of
 465 the main axes is close to vertical) in a single site. In a region
 466 such as northern Pakistan, with a complex tectonic history
 467 and strongly contrasted topography, the latter can be due to
 468 relief effects, or can correspond to tensors calculated on
 469 faults rotated during later movements. We will base our
 470 interpretation of the results largely on the main stress
 471 orientations of the “untilted” tensors.

472 3.3. Using the Multiple Inverse Method: Example of 473 Gilgit Area

474 [23] In the Gilgit area, we have collected data at five
 475 different sites, spread in a sector of 25 km along the Hunza
 476 and Gilgit rivers (Figure 3). All measurements were taken in
 477 dioritic rocks (Dainyor diorite) of the northern Kohistan
 478 Arc, south of the lineament of ultramafic rocks that sepa-
 479 rates the predominantly plutonic central Kohistan region
 480 from the northern volcano-sedimentary series (Figure 1)
 481 [*Le Fort and Pêcher, 2002*]. When merged together, these
 482 provide a set of 110 fault measurements from a tectonically
 483 and lithologically homogeneous area.

484 [24] Figure 4 shows the whole set of data projected in a
 485 Wulff net. A wide dispersion of fault orientations can be
 486 seen, suggesting a multisteps brittle deformation story. The
 487 plot clearly shows mixing of positive and negative rake
 488 values for striae of similar orientation, which implies

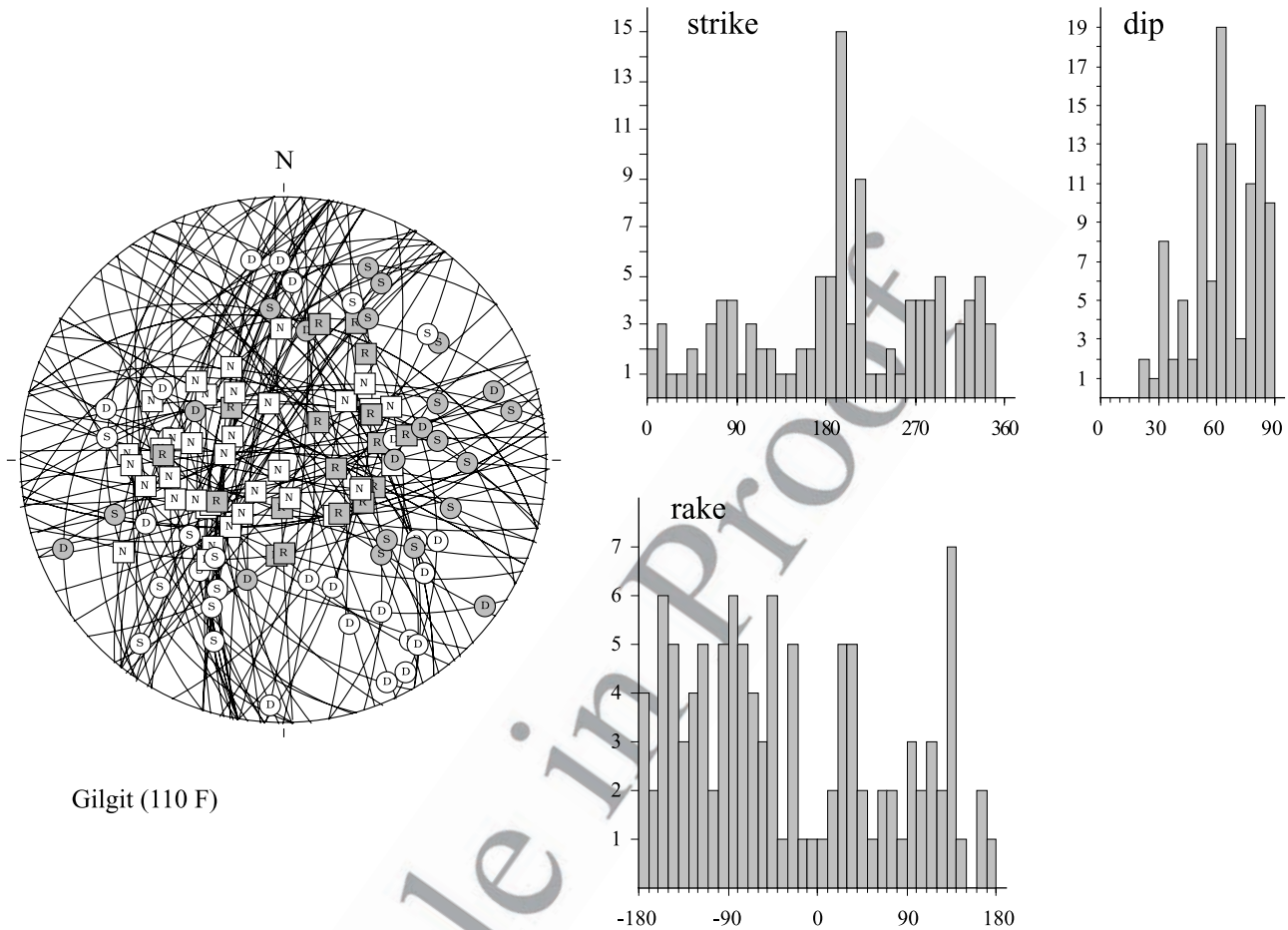
489 superposition of different stress states, possibly including
 490 stress axis inversion. When considering the histograms of
 491 fault strikes and dips (Figure 4), a preferred orientation of
 492 the faults (strike mode around 210° and dip mode around
 493 60° , i.e., steeply westward dipping faults) clearly appears,
 494 but the histogram of rakes again illustrates the great het-
 495 erogeneity of movements.

496 [25] To search for best fitting stress tensors, we use the
 497 miv4 software package of A. Yamaji et al. (Multiple Inverse
 498 Method Software Package, Freeware package, 2005, [http://](http://www.kueps.kyoto-u.ac.jp/~yamaji/PDS/indexe.html)
 499 www.kueps.kyoto-u.ac.jp/~yamaji/PDS/indexe.html). The
 500 σ_1 and σ_3 orientations obtained for 234 significant fault
 501 subsets are plotted Figure 5, with the color scale giving the
 502 value for the Φ ratio. Figure 5 shows clustering of the σ_1
 503 poles around a main orientation (N 190° E with a southward
 504 plunge), but the Φ ratio is poorly defined. A secondary
 505 cluster corresponds to steep σ_1 orientations. To discriminate
 506 possible tensors, we test the quality of the results while
 507 increasing the Φ ratio from 0 to 1 with steps of 0.1.

508 [26] This analysis yields nine possible tensors (Table 1),
 509 eight for a gently plunging σ_1 axis and one for steeply
 510 plunging σ_1 . An estimate of the quality of the result is given
 511 by the percentage of faults for which the deviation between
 512 the measured striae and the theoretical maximum shear
 513 stress on the plane (misfit angle α) is less than a given
 514 threshold value. As shown by *Liesa and Lisle* [2004], it is
 515 the most sensitive parameter to discriminate tensors. Those
 516 authors favor a misfit threshold of 12° . Tables 1 and 2
 517 consider misfit thresholds of 12° , 20° , 30° and 45° .

518 [27] Table 1 shows that similar stress orientations are
 519 obtained when increasing the Φ ratio from 0.1 to 0.8 (T1
 520 family, east–west σ_3 and north–south σ_1), while a tensor
 521 T2 (for $\Phi = 0.8$) has a distinct orientation (east–west σ_3 and
 522 steep σ_1). A detailed analysis identifies a single subset of
 523 faults that controls the calculation for all the tensors of the
 524 T1 family. To select the Φ ratio for the T1 tensor, we will
 525 rank the T1 solutions according to the number of faults with
 526 a striation close to the theoretical shear stress orientation.
 527 Accordingly, the tensors with a Φ ratio around 0.4 to 0.6
 528 best fit the data. To better fix the ratio, we recalculate the
 529 misfits for intermediate Φ values (the miv4 software allows
 530 only 0.1 steps). The largest number of faults compatible
 531 with T1 for a threshold of 12° is for $\Phi = 0.38$. Table 1 shows
 532 that tensor T2 (for $\Phi = 0.82$) which has an orientation
 533 distinct from T1 accounts for a smaller number of faults.
 534 The set of faults controlling the T2 tensor is clearly distinct
 535 (Table 2), however, and we can accept the T2 tensor as a
 536 well-defined distinct tensor. Thus, we can conclude that
 537 faults in this area record at least a two-stage brittle defor-
 538 mation history, corresponding to the two stress tensors T1
 539 and T2, even if slips corresponding to T2 are scarce.
 540 Additionally, a large amount of fault slips fit neither with
 541 T1 nor with T2. This result indicates that additional minor
 542 stress deviation must occur but has not been identified.

543 [28] The same superposition of tensors can be retrieved at
 544 the station scale, as illustrated in Figure 6: the two stations
 545 96-91 and 96-47 (Figure 3 for localization) share the same
 546 predominant set of steep west dipping faults. In station 96-
 547 91, they carry left-lateral strike-slip movements and are



Gilgit (110 F)

Figure 4. Faults in Gilgit area, northern Kohistan. Set of 110 fault/striation pairs. (left) Stereographic projection, Wulff net lower hemisphere. The sense of movement for each fault is given by the specific symbol used to plot the striae (N, R, S, and D for normal, reverse, sinistral, and dextral faults, respectively). The color of the symbol accounts for the sign of the rake of the slip, the rake λ being defined as the angle between the slip vector of the hanging wall relative to the footwall and the fault plane strike direction, so that $\lambda > 0^\circ$ for reverse faults and $|\lambda| \leq 90^\circ$ for sinistral faults [see Célérier, 1995], a gray symbol for positive rake (i.e., movement on the fault has a reverse component, indicating shortening deformation component), and a plain symbol for negative rake (i.e., movement on the fault has a normal component, extensional deformation component). (right) Histograms for fault strike (left-hand rule) and dip values and a histogram for striae rake values. Classes are of 10° .

548 coupled to a conjugate set of right-lateral faults. The
 549 predominant tensor calculated for this station (Table S1 in
 550 the auxiliary material) is close to T1 and can account for
 551 nearly all the faults. In station 96-47, the majority of the
 552 west dipping faults displays normal movements. The pre-
 553 dominant tensor is now close to T2, but a large residue of
 554 faults (mainly the south dipping reverse faults) is better
 555 explained by T1 than T2. In this station, scarce superposi-
 556 tion criteria would favor a relative chronology of T1
 557 followed by T2.

559 4. Results

560 4.1. Regional-Scale Average Stress Fields

561 [29] In areas with sufficient sites in a homogeneous
 562 structural unit, we have grouped the stations to estimate a

regional average stress field. Table 3 reports the results
 563 obtained by grouping the stations. It illustrates the wide
 564 range of stress tensors required by the data, either within a
 565 given area (implying superimposed successive stress states),
 566 or from one area to another (implying regional variations of
 567 the paleostress field). In Table 3, we have arbitrarily
 568 retained only the tensors which misfits less than 30° for at
 569 least 30% of the faults (except for Astor and Randu area,
 570 where less predominant tensors are needed to explain the
 571 data). For each area, two or three tensors are sufficient to
 572 explain the majority (up to 80% for Chalt area, 50 to 60%
 573 for other areas) of observed fault kinematics. Additional
 574 tensors can be calculated to improve the fit, but whatever
 575 the number of tensors, we keep a residue of $\sim 10\%$ unex-
 576 plained fault/striation pairs. Considering the tensors required to
 577 decrease the residue (tensors not reported in Table 3) two
 578

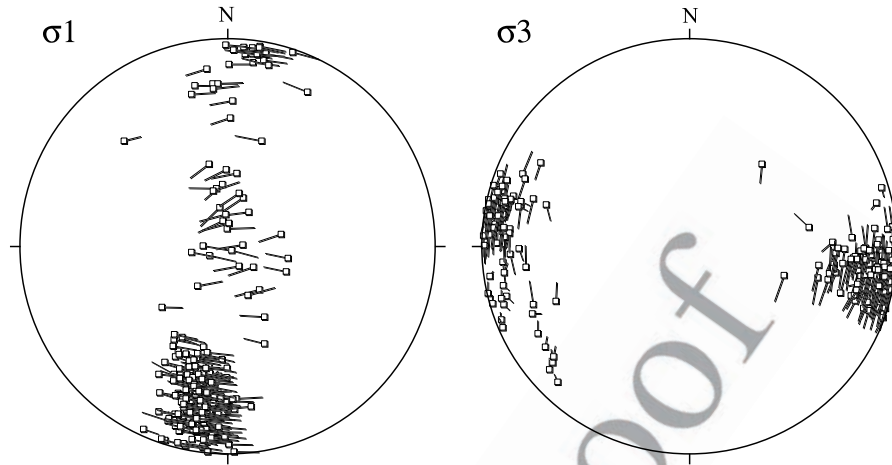


Figure 5. Gilgit area, results from the multiple inverse methods (software package mim5-miv4 of A. Yamaji et al., Multiple Inverse Method Software Package, Freeware package, 2005, locator-type="URL"><http://www.kueps.kyoto-u.ac.jp/~yamaji/PDS/indexe.html>); 224 points (from a 60,000 nodes grid) having a significant number of σ_1 or σ_3 orientations tied to them, plotted lower hemisphere, equal-area projections. (left) Square symbols define the σ_1 orientations, the bars attached on the squares show the plunge and azimuth of σ_3 axis (the shorter the lines, the steeper the corresponding stress axes). (right) Squares define σ_3 orientations; the bars show the plunge and azimuth of σ_1 axes.

579 cases are common: (1) they are tensors having different
580 principal stress orientations as compared to the retained
581 tensors but accounting for only a small number of data (we
582 have neglected these) and (2) they are tensors with similar
583 principal stress axis orientations as those reported, but with
584 a different Φ ratio. These probably reflect progressive
585 changes in the strain regime, from compression to wrench
586 or from wrench to extension.

587 [30] Main results are presented in two ways: using a
588 tectonic regime plot [Armijo et al., 1982; C el erier, 1995]
589 and as a map representation of the projections of σ_1 and σ_3
590 orientations onto the horizontal plane.

591 [31] In the tectonic regime plot (Figure 7), only tensors
592 with one vertical or close to vertical axis (i.e., “untilted”
593 tensors) can be plotted. This plot distinguishes extensional,
594 wrench and compressional strain regimes, on the basis of
595 which of the principal stress axes is vertical. West of the

Raikhot fault, wrenching is the most common strain regime. 596
It corresponds mainly to steep strike-slip faults. In the 597
Besham, Nanga Parbat and Dasso dome areas, extension 598
(mainly normal faults) is predominant. Extension has also 599
been evidenced in all other main tectonic units. In contrast, 600
records of compressional strain (mainly reverse faults) are 601
rare. The plot also shows the variability of the Φ ratio 602
(varying from 0.1 to 0.8) in a single area (as already 603
demonstrated for the Gilgit test area) or from one area to 604
another. Such variability reveals instability of the stress 605
state, with rapid shifting from one type of stress regime to 606
another through permutation of the σ_1 – σ_2 or σ_2 – σ_3 axes, 607
for high or low values of Φ , respectively. 608

[32] The map (Figure 8) shows the main tensor orienta- 609
tions obtained for each area as a horizontal projection of the 610
principal stress axes. For the sake of clarity, only two 611
tensors are shown for each region. In most cases, we 612

t1.1 **Table 1.** Main Tensors Coming Out From the Set of 110 Faults Measured in Gilgit Area^{a,b}

t1.2	Tensor	Φ	σ_1	σ_3	$\alpha < 12^\circ$ (%)	$\alpha < 20^\circ$ (%)	$\alpha < 30^\circ$ (%)	$\alpha < 45^\circ$ (%)
t1.3	T1	0.1	36/196	14/096	18.2	24.5	31.8	46.4
t1.4	T1	0.2	41/196	05/101	19.1	26.4	34.5	49.1
t1.5	T1	0.3	33/195	10/099	22.7	30.9	38.2	51.8
t1.6	T1	0.4	33/193	00/103	24.5	31.8	42.7	48.2
t1.7	T1	0.38	33/193	00/103	26.4 (29 f)	31.8	41.8	49.1
t1.8	T1	0.5	28/193	04/101	23.6	36.4 (40 f)	44.5 (49 f)	50.9
t1.9	T1	0.6	13/190	02/099	18.2	33.6	40.9	51.8
t1.10	T1	0.7	19/187	09/280	18.2	30.0	38.2	50
t1.11	T1	0.8	18/190	10/097	18.2	28.2	40.1	54.5
t1.12	T2	0.8	78/124	11/277	15.5	24.5	33.6	50
t1.13	T2	0.82	78/124	11/277	15.5 (17 f)	25.5 (28 f)	33.6 (37 f)	50

t1.14 ^aAxis orientations given as plunge/plunge direction.

t1.15 ^bFor α the percentage of faults for which the misfit angle between the observed and calculated striae is less than 12° , 20° , 30° , and 45° .

t2.1 **Table 2.** Number of Fault Movements Measured in the Gilgit Area That Can Be Explained by T1 and T2 or Indifferently by T1 and T2

t2.2	Misfit Threshold	Fitting Only With T1	Fitting Only With T2	Fitting With Both T1 and T2	Total
t2.3	<12° ($\Phi = 0.38$)	24 (21.8%)	12 (10.9%)	5 (4.5%)	41 (37.7%)
t2.4	<12° ($\Phi = 0.5$)	20 (18.2%)	11 (10.0%)	6 (5.5%)	37 (33.6%)
t2.5	<20°	21 (19.1%)	9 (8.2%)	19 (17.3%)	49 (44.5%)
t2.6	<30°	21 (19.1%)	9 (8.2%)	26 (23.6%)	58 (52.7%)
t2.7	<45°	14 (12.7%)	13 (11.8%)	42 (38.2%)	69 (62.7%)

613 retained the two tensors accounting for the largest number
 614 of observed fault movements (Table 3). When these two
 615 tensors were nearly parallel and mainly differed by their Φ
 616 ratio, we display the most important tensor with significant-
 617 ly different orientation, if any.

[33] A number of features are particularly noticeable in 618
 Figure 8. First, the plunge of σ_3 is predominantly low, that 619
 is, wrench or extensional deformation predominates. The 620
 predominantly low plunge of σ_3 axes contrasts with the 621
 greater observed variability for the plunges of σ_1 . Second, 622

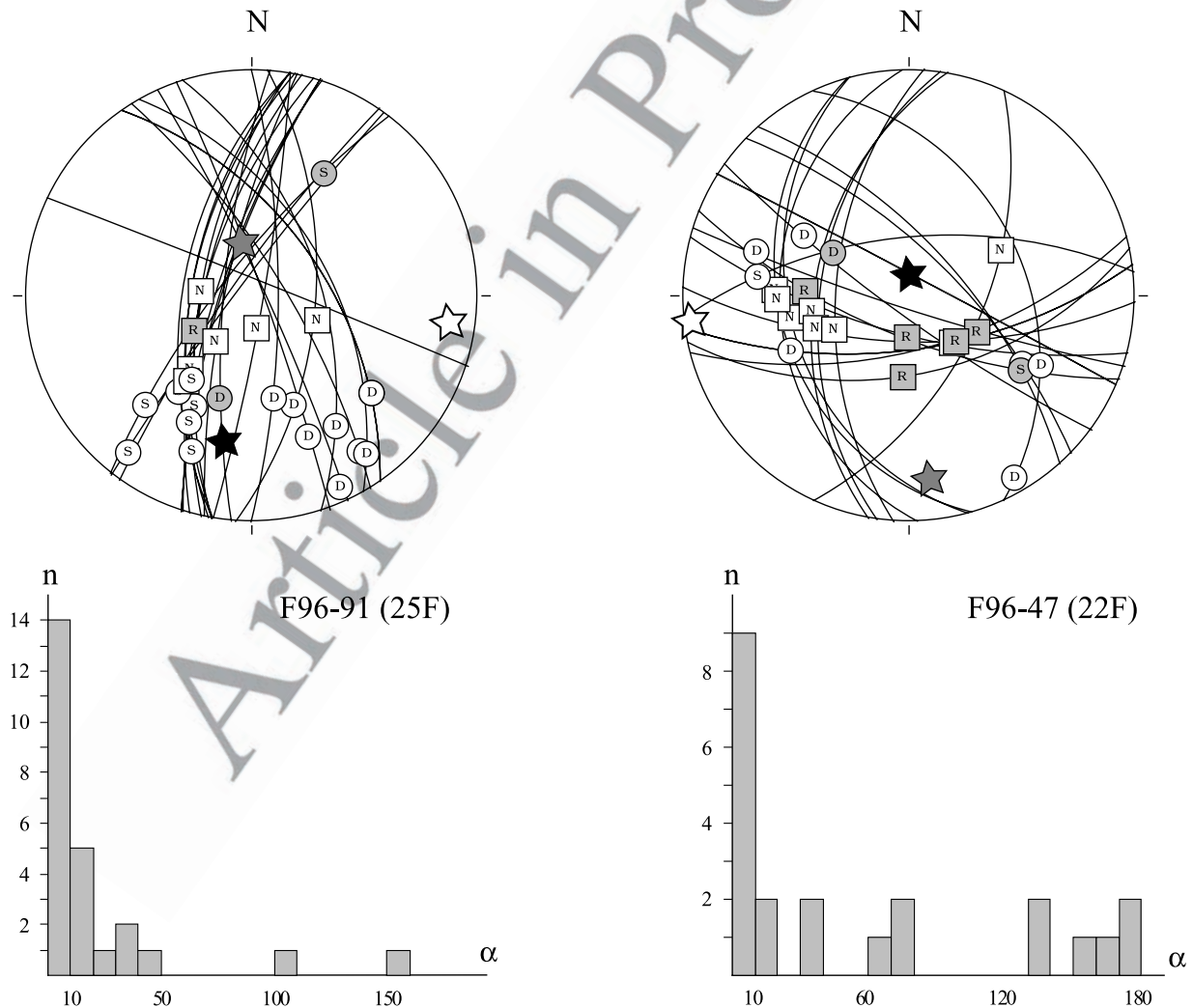


Figure 6. Sites 96-91 and 96-47 from Gilgit area (see Figure 3 for location). Projection of the fault/striation pairs, Wulff net, lower hemisphere (same conventions as Figure 4). Black star and plain star indicate positions of σ_1 and σ_3 calculated using the miv4 software package of A. Yamaji et al. (Multiple Inverse Method Software Package, Freeware package, 2005, <http://www.kueps.kyoto-u.ac.jp/~yamaji/PDS/indexe.html>). Grey star indicates σ_2 . Histograms show misfit angles α between the striae and the theoretical shear stress on the fault, for classes of 10°.

t3.1 **Table 3.** Main Tensors Coming Out From Grouped Stations^a

t3.2	Tensor	Φ	σ_1	σ_3	$\alpha < 12^\circ$ (%)	$\alpha < 20^\circ$ (%)	$\alpha < 30^\circ$ (%)	$\alpha < 45^\circ$ (%)
t3.3				<i>Astor (218F) Nanga Parbat Cover (Metasediments)</i>				
t3.4	T1	0.07	22/266	33/011	15	22	30	35
t3.5	T2	0.42	51/272	02/005	16	22	26	34
t3.6	T3	0.52	83/276	00/006	8	17	24	33
t3.7	All tensors				26	38	46	53
t3.9				<i>Besham (88F) Himalayan Gneiss</i>				
t3.10	T1	0.72	69/219	19/014	17	23	33	42
t3.11	T2	0.12	76/115	01/207	19	25	31	39
t3.12	T3	0.55	42/139	31/016	18	24	30	33
t3.13	All tensors					35	43	50
t3.15				<i>Central Kohistan (141F) Chilas Gabbro-Norite Complex</i>				
t3.16	T1	0.82	03/310	24/041	18	29	38	46
t3.17	T2 ^b	0.28	14/344	10/077	21	29	37	44
t3.18	T3 ^b	0.28	06/353	83/199	15	24	31	37
t3.19	All tensors				39	51	64	71
t3.21				<i>Chalt (95F) Chalt Volcanics</i>				
t3.22	T1	0.32	07/038	03/129	28	34	41	47
t3.23	T2	0.05	00/241	83/149	22	27	37	43
t3.24	T3 ^c	0.25	80/049	10/234	22	28	33	39
t3.25	All tensors				55	70	80	87
t3.27				<i>Chilas (241F) Chilas Gabbro-Norite Complex</i>				
t3.28	T1	0.8	77/124	11/271	20	27	34	44
t3.29	T2	0.93	06/000	14/269	18	26	34	47
t3.30	T3	0.75	82/206	08/019	9	15	21	28
t3.31	T4	0.4	07/252	03/342	8	14	19	25
t3.32	All tensors				33	46	57	70
t3.34				<i>Dassu Dome (87F) Karakorum Orthogneiss</i>				
t3.35	T1	0.18	86/045	04/198	20	33	45	51
t3.36	T2	0.4	80/199	09/356	17	32	44	48
t3.37	All tensors				30	46	57	61
t3.39				<i>Deosai E (160F) Ladakh Plutonites and Volcanites</i>				
t3.40	T1	0.55	71/108	13/235	16	24	31	37
t3.41	T2	0.21	51/241	37/040	18	21	30	37
t3.42	T3	0.15	56/239	33/66	14	20	31	39
t3.43	All tensors				39	49	59	66
t3.45				<i>Gilgit (110F) Dainyor Diorite</i>				
t3.46	T1	0.5	28/193	04/101	24	36	45	51
t3.47	T2	0.8	78/124	11/277	16	25	34	51
t3.48	All tensors				34	45	53	63
t3.50				<i>Hunza (85F) Southern Karakorum Metasediments</i>				
t3.51	T1	0.4	17/086	05/177	24	32	41	44
t3.52	T2	0.18	07/085	82/250	21	32	40	44
t3.53	T3	0.4	87/286	01/177	21	25	32	47
t3.54	All tensors				44	55	64	71
t3.56				<i>Karakorum N (122F) Northern Karakorum Metasediments</i>				
t3.57	T1 ^d	0.3	10/350	06/259	17	26	36	44
t3.58	T2 ^d	0.8	85/074	05/253	14	22	30	45
t3.59	T3	0.1	12/344	68/107	18	25	30	37
t3.60	All tensors				35	43	51	63
t3.62				<i>Nanga Parbat (182F) Nanga Parbat Core (High-Grade Gneiss and Migmatites)</i>				
t3.63	T1	0.75	64/115	06/217	21	29	39	48
t3.64	T2	0.5	45/115	06/211	15	25	36	50

Table 3. (continued)

t3.65	Tensor	Φ	σ_1	σ_3	$\alpha < 12^\circ$ (%)	$\alpha < 20^\circ$ (%)	$\alpha < 30^\circ$ (%)	$\alpha < 45^\circ$ (%)
t3.66	T3	0.25	62/028	27/191	18	28	34	43
t3.67	All tensors				47	61	69	76
t3.69			<i>Randu (136F) Ladakh, Askor Amphibolites</i>					
t3.70	T1	0.66	74/075	12/212	14	22	32	40
t3.71	T2	0.5	42/152	09/054	17	22	27	33
t3.72	All tensors				30	41	51	63

^aAxis orientations given as plunge/plunge direction. Percentage of faults for which the misfit angle between the observed and calculated striae is less than 12° , 20° , 30° , and 45° . For each area, the tot gives the percentage of fitting data when taking into account all the tensors (two to four tensors) for the given area.

t3.73
t3.74 ^bMainly radial extension, two preferred orientations well defined by specific faults.

t3.75 ^cT3 recalculated on a residue of 42 faults explained neither by T1 nor T2.

t3.76 ^dPossible inversion of σ_1 and σ_2 , but with each tensor well defined by specific faults.

623 stress fields show strong spatial variability at the map scale.
624 This is especially evident from the σ_3 orientations, which
625 show clearly distinct patterns to the west and east of Nanga
626 Parbat. The western limit of Nanga Parbat (i.e., the MMT
627 reactivated by the Quaternary Raikhot fault) thus appears as
628 a first-order tectonic contact, between two crustal blocks
629 with a different tectonic history or mechanical behavior. To
630 the east, in a zone including the Nanga Parbat anticline, but
631 also the Deosai Plateau, the Indus valley north of it and the
632 Dassu dome, averaged σ_3 orientations are predominately
633 oriented NNE–SSW to NNW–SSE, whereas to the west, in
634 Kohistan and the western Karakorum, the orientation of σ_3
635 is predominantly E–W. Third, most tensors indicate hori-
636 zontal extension (i.e., are characterized by steeply dipping
637 σ_1), especially in the eastern block, while the region is in a
638 convergent kinematic regime: Himalayan convergence has
639 averaged 20 mm a^{-1} [e.g., *DeCelles et al.*, 2002; *Guillot et*
640 *al.*, 2003] since Eocene collision up to the present-day, and
641 up to 20 mm a^{-1} shortening is currently recorded in the
642 central Himalaya [*Larson et al.*, 1999; *Paul et al.*, 2001;
643 *Jouanne et al.*, 2004].

644 4.2. Site-to-Site Variation of the Paleostress Orientations

645 [34] For each site, we have processed the set of fault data
646 following the same approach as above for the stations
647 grouped per zone. To ensure more robust stress determi-
648 nations, we have systematically test back the assumed
649 tensors on the set of faults to determinate for each fault
650 the misfit between the theoretical and observed striae
651 orientation, and clearly individualize the faults fitting the
652 tensor. In many stations, more than one tensor is required to
653 explain the observed slip movements. Only the two best
654 defined ones have been retained, the others being con-
655 strained by a too low number of faults. Because of the
656 large number of data, only a few characteristic fault distri-
657 bution patterns are given hereafter (Figure 9, localization of
658 the sites, Figure 3), the results for all the stations being
659 summarized in Table S1.

660 [35] Station 06-13 (Astor valley, eastern Nanga Parbat
661 cover, Figure 9a) is an example of the most common
662 pattern: no clear preferred orientation of the faults, slip best
663 explained by at least two tensors, each tensor T1 and T2
664 being defined by a significant amount of specific faults,

even if part of the observed striae can be explained equally 665
well by both tensors. Figure 9a shows the faults compatible 666
with T1 or T2 with misfits $< 30^\circ$: 10 faults are common to 667
both tensor, 11 faults fit only with T1 and 8 only with T2; 668
for a threshold of 12° , only 2 faults are common to both 669
tensors, but there are still 10 and 7 faults compatible with 670
T1 and T2, respectively. In this station, striae superposition 671
on some faults indicates that T1-related slips probably 672
occurred prior to T2-related slips. 673

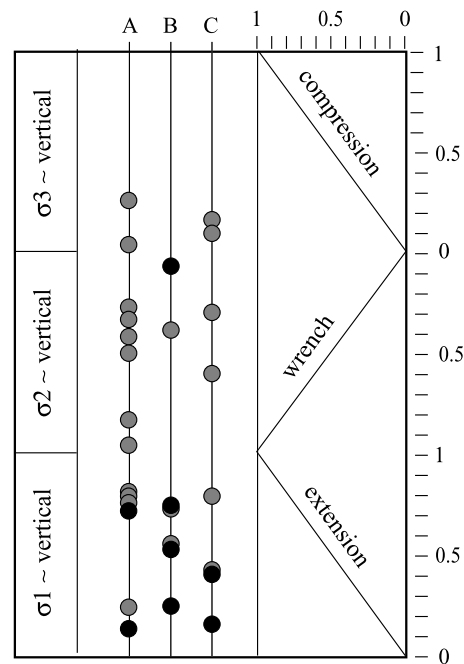


Figure 7. Grouped sites. Tectonic regime summary shows the strain regime. Horizontal and vertical scales indicate Φ ratio value (see text). Vertical lines are A for west of the Raikhot fault, in Kohistan (gray symbols) and Besham area (black symbols); B for east of the Raikhot fault, in Nanga Parbat (black symbols) and Ladakh; and C for north of the MKT, in Karakorum (black symbols: Braldu-Dassu area).

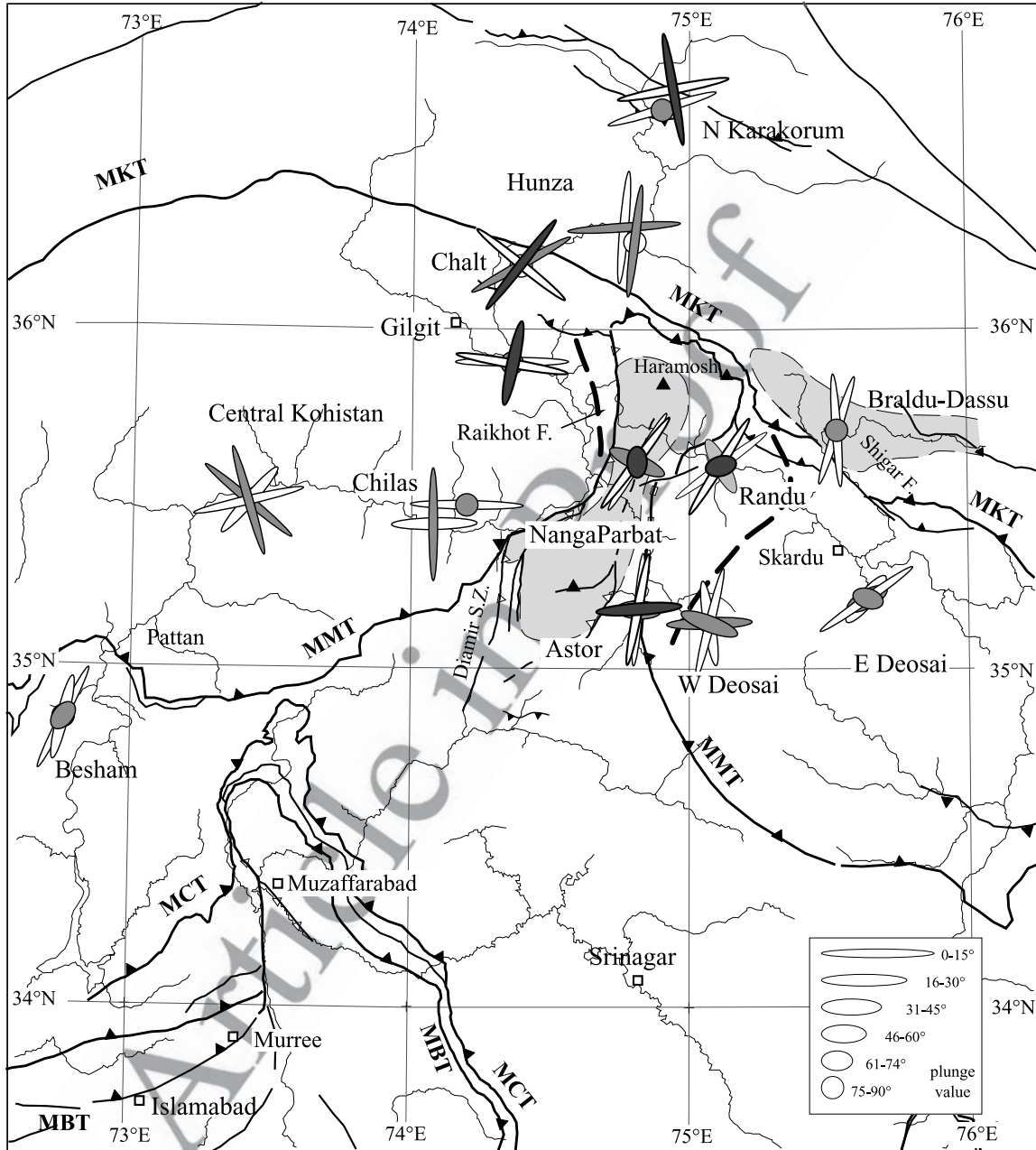


Figure 8. Regional stress orientations in northern Pakistan. Tensors are calculated by merging faults measured in 4 to 11 individual outcrop-scale sites (see Figure 3). Each stress axis is indicated by an ellipse: the great axis of the ellipse gives the azimuth of the principal stress axis, the shape of the ellipse its plunge (classes of 15°). For each area, only the two best tensors (see text and Table 3) are shown. For T1, σ_1 in black, σ_3 thick plain symbol; for T2, σ_1 in gray, σ_3 light plain symbol. Shaded area indicates zones of Plio-Quaternary very active exhumation; thick dashed line indicates eastern morphological limit of the Nanga Parbat area.

674 [36] Station 00-67 (Deosai plateau, Kohistan, Figure 9b)
 675 illustrates another frequent situation: despite the low number
 676 of measured faults, it seems possible to define two
 677 tensors T1 and T2. If we accept misfits of 30° , 3 faults are
 678 common to both tensors, 7 faults fit only with T1 and 7 only
 679 with T2; for a threshold of 12° , no faults are common to

both tensors, but there are still 5 and 6 faults compatible 680
 with T1 and T2, respectively. In this station, faults compat- 681
 ible with T1 have chlorite-epidote coating, and are probably 682
 older than the “colder” faults corresponding to T2 that do 683
 not show such coating. This station thus provides evidence 684

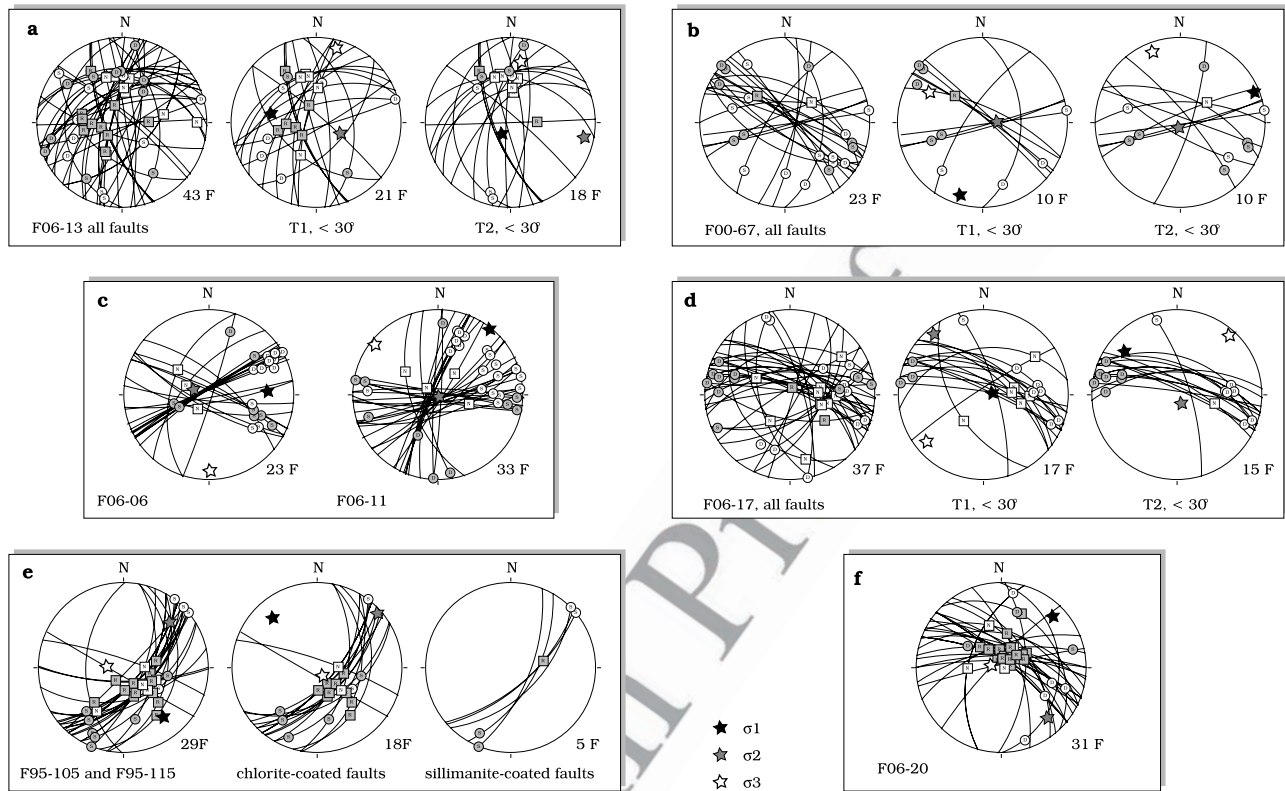


Figure 9. Fault/striae patterns from some typical sites. Stereographic projection, Wulff net lower hemisphere (same conventions as Figure 4). Localization of the sites is given Figure 3.

685 of an older NNE–SSW compression, which has not been
 686 evidenced in this area when grouping the stations in zones.
 687 [37] The stations 06-06 and 06-11 (Hunza and Chalt area,
 688 respectively, Figure 9c) illustrate the simple case of two
 689 conjugate sets of strike-slip faults. In this case, a single
 690 tensor can account for most of the faults (74% and 82% of
 691 the faults, respectively, for a maximum misfit of 30°). The
 692 calculated tensor is in good agreement with the regional
 693 tensor calculated for both areas. Nevertheless, normal faults
 694 crosscutting strike-slip faults in these stations indicate here
 695 too the superposition of a second tensor with steeply
 696 plunging σ_1 .

697 [38] Station 06-17 (Kohistan, Figure 9d) is a case where
 698 the stress tensor is poorly defined by one predominant set of
 699 faults. Two tensors can be defined, corresponding to a
 700 permutation of σ_1 and σ_2 . If we consider misfits $< 30^\circ$,
 701 only 6 and 5 faults are specific to T1 and T2, respectively,
 702 and 11 faults can be explained indifferently by T1 and T2.
 703 Such a pattern suggests instability in the stress state or in the
 704 inversion. Striae superposition observed in the field, how-
 705 ever, support two distinct episodes, with T1 preceding T2.

706 [39] Figure 9e does not correspond to a single station, but
 707 groups faults measured along the upper part of the Fairy
 708 Meadow road (Tato valley, stations 95-105 and 95-115), in
 709 high-grade migmatitic gneiss of the Nanga Parbat core,
 710 close to its western limit. In this area, we observe mylonitic
 711 structures striking predominantly NNE–SSW, i.e., parallel
 712 to the Nanga Parbat axis and to the Quaternary Raikhot

713 fault. The oldest structures are left lateral shear zones with
 714 S-C type fabrics. As discussed by *Argles and Edwards*
 715 [2002], they predate Neogene Nanga Parbat anticline forma-
 716 tion, as well as the high-temperature (sillimanite +
 717 cordierite anatexis) Neogene metamorphism observed in
 718 the core of the anticline. They probably trace southward
 719 thrusting of the Kohistan-Ladakh zone on top of the
 720 Himalayan gneisses. The S-C fabric is reactivated as silli-
 721 manite-coated strike-slip faults developed during or just
 722 after the peak of Neogene high-temperature metamorphism,
 723 and subsequently as chlorite coated reverse faults during the
 724 Pliocene-Quaternary temperature decrease (biotite Ar/Ar
 725 ages less than 5 Ma [*Schneider et al.*, 2001]). It is possible
 726 to calculate a tensor on the bulk set of fault, but this is
 727 meaningless given the clear temporal evolution observed in
 728 the field. It is more useful to consider the tensor calculated
 729 using only the chlorite coated reverse faults, which provides
 730 a single tensor T1, compatible with westward thrust com-
 731 ponent on the Raikhot fault, which corresponds to the last
 732 steps of the NNW–SSE Nanga Parbat shortening. The
 733 sillimanite-coated strike-slip faults correspond to another,
 734 older tensor, the orientation of which is undeterminable.

735 [40] Last, Figure 9f shows the faults of station 06-20,
 736 measured at the tip of the Murree syntaxis, just north of
 737 the MBT, in Lesser Himalaya metasediments. The stress
 738 tensor cannot be precisely fixed, but the σ_1 orientation
 739 (NNE–SSW to NE–SW) is clearly compatible with the

740 focal mechanism of the Balakot earthquake (Global CMT
741 Catalog).

742 [41] Altogether, analyzing the data on a site per site basis
743 reveals a complex and heterogeneous pattern. Most stations
744 require more than one tensor to explain their set of measure-
745 ments. The map in Figure 10 shows a simplified image of
746 the results, as only the orientation of the tensor accounting
747 for the largest number of faults has been reported for each
748 site. Because of this choice, the map mixes asynchronous
749 data: the fact that several sites in the same region show
750 different stress orientations more probably reflects a differ-
751 ent imprint of subsequent tensors in the considered sites,
752 rather than a sharp lateral discontinuity in stress regime.
753 Nevertheless, the map confirms and completes the larger-
754 scale results shown Figure 8.

755 [42] The Nanga Parbat spur again shows up as a domi-
756 nant boundary in the stress regime, as it does structurally
757 and geomorphologically. In Nanga Parbat and the area
758 immediately to the east, three different situations can
759 predominate depending on the site: (1) extension parallel
760 to the anticlinal axis of Nanga Parbat (σ_1 vertical, σ_3 S–N
761 to SSW–NNE), (2) shortening perpendicular to the fold
762 axis (σ_1 WNW–ESE to W–E, σ_3 SSW–NNE to S–N) and
763 (3) in several sites, σ_3 roughly parallel to the anticlinal axis
764 but intermediate plunges of σ_1 . This variation is most easily
765 explained by rotation of the fault sets, with a rotation axis
766 parallel to the anticlinal axis. These features thus fit with a
767 fold growing in a strain regime characterized by shortening
768 parallel to the belt, as also suggested by the pattern of
769 geochronological ages [Schneider *et al.*, 2001].

770 [43] We note that the zone displaying this pattern has a
771 larger extension than the zone of unroofed Himalayan
772 gneisses, i.e., the Nanga Parbat spur bounded by the
773 MMT trace. To the east, it includes a strip of Ladakh Arc
774 formations, of approximately the same width as the Nanga
775 Parbat spur itself. The eastern limit of this strip is not well
776 defined (Figure 10), but approximates the morphological
777 limit of Nanga Parbat. It corresponds to the eastern end of
778 the deep Indus gorge, which is characterized by high
779 incision rates [Burbank *et al.*, 1996; Leland *et al.*, 1998],
780 and to the eastern limit of the Astor river gorge, which is
781 followed to the east by the Dassu-Deosai zone of much
782 smoother relief. West of the Nanga Parbat spur, we find this
783 characteristic stress pattern (SSW–NNE σ_3 , e.g., station 95-
784 153, Table S1 in the auxiliary material) only in a narrow
785 corridor of <2 km width west of the northern ending of the
786 Sassi-Raikhot fault (i.e., the Quaternary reactivated MMT).

787 [44] Altogether, the stress pattern in and around Nanga
788 Parbat is consistent with a large zone of vertical extrusion in
789 an asymmetrical west vergent dome. The Himalayan middle
790 crust currently extrudes in the western part of the dome, the
791 Nanga Parbat anticlinorium itself. The structural asymmetry
792 may correspond to a transient state in a system where the
793 Nanga Parbat fold progressively widens to the east, but we
794 have currently no evidence for such an evolution. Another
795 possibility is that it is due to mechanical weakening by the
796 extrusion of Himalayan gneiss on the western flank of the
797 massif after the erosion of the hanging wall, and amplifica-
798 tion of the fold by a feedback process between erosion,

exhumation and rock uplift (as suggested by Zeitler *et al.* 799
[2001a, 2001b]). Cooling ages indicate that ductile displace- 800
ment on the reverse shear zones bordering the Nanga Parbat 801
pop-up on both sides (i.e., the Diamir and Rupal shear 802
zones) ceased before the onset of vertical ductile flow in the 803
core of the massif (2.3 Ma versus 1 Ma [Schneider *et al.*, 804
2001]), supporting the hypothesis of progressive strain 805
localization. 806

[45] Southward from Nanga Parbat, we do not have 807
sufficient data to fix the limit between a Kohistan-type 808
stress regime (as observed, for instance, in the Chilas area: 809
roughly N–S σ_1 and E–W σ_3) and Nanga Parbat-type 810
stress regime (steep or E–W σ_1 and N–S σ_3). Only one site 811
is located directly south of the Nanga Parbat spur, in the 812
Nangi Mali area [Pêcher *et al.*, 2002]. Here, ductile struc- 813
tures (thrusts and folds) strike parallel to the Himalayan 814
trend (WNW–ESE), but we obtain a stress tensor with the 815
same orientation as in the main Nanga Parbat structure, 816
indicating shortening parallel to the belt. 817

[46] On both sides of the Nanga Parbat zone as defined 818
above, in Ladakh–Deosai and Kohistan as well as in the 819
Karakorum, wrench strain is predominant (σ_1 and σ_3 820
horizontal). It marks the bulk Himalayan convergence, 821
with a σ_1 orientation close to north–south (consistent 822
with shortening more or less parallel to the convergence 823
orientation) and a σ_3 orientation close to east–west 824
(indicating lateral extrusion perpendicular to the conver- 825
gence orientation). 826

5. Discussion 828

[47] A major challenge to paleostress studies in multiple 829
deformed areas is establishing an absolute or even a relative 830
chronology of the stress events. Field observations can help 831
to constrain this chronology, for instance, by considering 832
fault intersection criteria, superposition of striae, or the 833
mineralogical nature of the fault gouge. In the sites we 834
studied in northern Pakistan, however, we found only few 835
unambiguous field criteria to establish a relative chronology 836
of the faults. Moreover, the relation between a set of faults 837
and any particular tensor might be ambiguous, as the same 838
fault/striae pair can be activated by more than one tensor. 839
Absolute dating of the minerals crystallized on the fault 840
plane or in the fault gouge could, in principle, constrain the 841
age of the faults. In northern Pakistan, however, appropriate 842
minerals are rare: most faults are dry (i.e., no minerals are 843
developed on the fault plane, or minerals have been dis- 844
solved) or show mainly argillaceous products. Chlorite- 845
calcite-epidote or chlorite-quartz assemblages are rare and 846
micaceous coats even more so. In addition, we frequently 847
observed indications for fluid circulation (mostly in the 848
form of extension veins superimposed on striations or 849
secondary crystallization), which contaminate any mineral 850
that may correlate with fault displacement. Nevertheless, 851
despite the difficulty of dating the events directly from 852
individual fault observations, the timing of stress events and 853
brittle deformation in northern Pakistan can be bracketed 854
indirectly by the more easily dated ductile tectonics and by 855

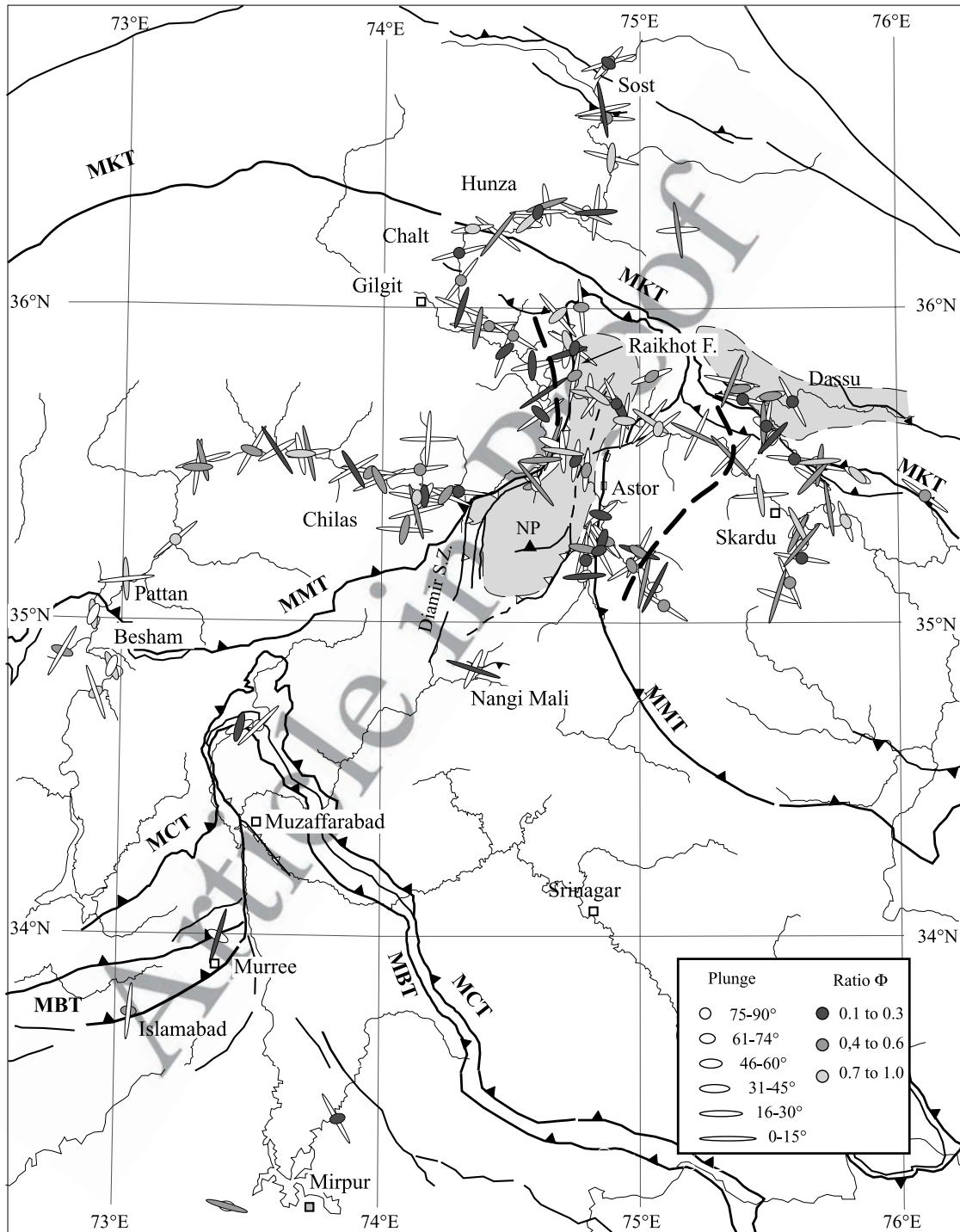


Figure 10. Paleostress orientations from individual site measurements. In each site, only the tensor with the largest number of fitting faults is plotted. Stress is represented by an ellipse, the great axis of which shows the principal stress axis orientation, whereas its ellipticity represents the plunge (from nearly horizontal, high ellipticity, to nearly vertical, circle). Shape ratio Φ (low, medium, high) is indicated by the color of the σ_1 ellipse; σ_3 , plain ellipse. Thick dashed line indicates eastern morphological limit of the Nanga Parbat area (see text for discussion).

856 the ages of exhumation, as provided by thermochronolog- 915
857 ical data. 916

858 [48] Concerning the two domains evidenced at a regional 917
859 scale and separated by the Raikhot fault, the different 918
860 observed stress patterns probably reflect two different stages 919
861 of the tectonic activity, of different ages. East of the Raikhot 920
862 fault, most of the Nanga Parbat pop-up anticline was in the 921
863 ductile deformation field up to recently, as indicated by 4 to 922
864 11 Ma monazite U/Pb ages obtained on the high-grade 923
865 migmatitic gneisses [Smith *et al.*, 1992], 1 to 5 Ma Ar/Ar 924
866 cooling ages of biotite obtained in these gneisses [Trelor *et al.*, 2000; Schneider *et al.*, 2001], the intrusion of granites as 925
867 young as 1 Ma [Zeitler *et al.*, 1993], and the shallow (5– 926
868 6 km) present-day brittle-ductile transition as revealed by 927
869 seismic investigations [Meltzer *et al.*, 2001]. Given the high 928
870 (60°C km⁻¹) geothermal gradient in the upper crust of the 929
871 western Himalaya [Winslow *et al.*, 1994] and rates of 930
872 exhumation that reached 5–10 mm a⁻¹ over the past 3 Ma 931
873 [Schneider *et al.*, 1999], we expect rocks currently outcrop- 932
874 ping within the Nanga Parbat core to have passed the brittle- 933
875 ductile transition less than a few million years ago. Thus, 934
876 brittle extension in this area must reflect mainly the recent 935
877 (late Pliocene and Quaternary) stress state. In the Dasu 936
878 dome area, high-temperature metamorphism in the core of 937
879 the dome took place at 6–7 Ma, from U/Pb ages on 938
880 monazite [Smith, 1993], at temperatures ≥ 750°C [Rolland 939
881 *et al.*, 2001], and it cooled by exhumation through the Ar- 940
882 Ar closure temperature in biotite at ~5 Ma [Searle *et al.*, 941
883 1989]. Thus the N–S to NNE–SSW extensional stress 942
884 observed in these areas cannot be older than Plio-Pleistocene, 943
885 and is associated with the exhumation of Nanga 944
886 Parbat and the Karakorum domes. The stress tensors 945
887 evidenced here correspond to recent deformation stages, 946
888 without tectonic inheritance from older (pre-Pliocene) 947
889 phases. 948

891 [49] West of the Raikhot fault, most of Kohistan appears 949
892 to be tectonically stable and characterized by low exhumation 950
893 rates, as indicated by zircon fission track ages (closure 951
894 temperature ~240°C [e.g., Brandon *et al.*, 1998]) ranging 952
895 from 15 to ~50 Ma [Zeitler, 1985; Zeilinger *et al.*, 2007]. In 953
896 this region, the stress field deduced from the brittle deformation 954
897 features is dominated by N–S shortening in a 955
898 wrench strain regime. This shortening orientation is coherent 956
899 with the bulk India-Asia convergence orientation, but 957
900 not with the current NE–SW belt-scale shortening, as 958
901 indicated by the present-day seismicity. It does fit with 959
902 south vergent stacking of the Karakorum and Himalayan 960
903 units, where ductile synmetamorphic nappe emplacement 961
904 ended around 16 Ma [Fraser *et al.*, 2001]. Thus, the tensor 962
905 for Kohistan appears to correspond to the average regional 963
906 stress field during the Miocene or earlier, rather than to Plio- 964
907 Pleistocene deformation. It is oblique to the MKT, implying 965
908 transpression on this structure and explaining the right- 966
909 lateral strike-slip movement observed on it. 967

910 [50] In fact, multistage brittle deformation has been 968
911 recorded in nearly all the sites, as indicated by the fact that 969
912 more than one tensor is required to explain the set of striated 970
913 fault planes. Figure 10 shows only the most clearly 971
914 expressed tensor for each site (i.e., the tensor explaining

the largest number of faults movements) and thus provides a 915
distorted image of the paleostress pattern as it probably 916
mixes asynchronous tensors. A clearer site-to-site compar- 917
ison arises when plotting separately the tensors compatible 918
either with shortening, wrench or extensional deformation 919
(corresponding to the σ_3 , σ_2 , σ_1 axis, respectively, being 920
vertical or nearly vertical). For this analysis, we retained for 921
each site the tensor(s) for which the three main axes were 922
less than 20° away from vertical or horizontal 923
(corresponding to untilted or slightly tilted tensors). 924

5.1. Compressional Stress Fields 925

[51] Figure 11a shows the σ_1 orientation for all sites in 926
which we determine a tensor with σ_3 close to vertical, and 927
both σ_1 and σ_2 close to horizontal. For each site, only σ_1 928
has been plotted, the color of the ellipse corresponds to the 929
 Φ ratio (from $\Phi > 0$, compressional regime, to $\Phi = 0$, 930
transition to wrench regime). Only few sites retain a record 931
of compressional tectonics. Nevertheless, it is possible to 932
recognize the superposition of two (or possibly three) main 933
orientations: 934

[52] WNW–ESE compression, parallel to the belt, is 935
recorded on both sides of Nanga Parbat in Kohistan and 936
less clearly in Ladakh. This stress field is consistent with 937
initiation of the Nanga Parbat transverse fold by doming 938
during upper Miocene times [Schneider *et al.*, 2001] and its 939
subsequent evolution as a pop-up structure. We have not 940
been able to recognize this stress tensor in the Nanga Parbat 941
or its boundaries itself. The reasons are that the Nanga 942
Parbat core was still in the ductile field at this time, whereas 943
faults that were created or activated by E–W compression 944
within the outer sequence will have been rotated or reactivated 945
during subsequent fold amplification. 946

[53] NNE–SSW to NE–SW compression, perpendicular 947
to the local orientation of the Himalayan arc, is recorded 948
mainly east of Nanga Parbat, in Ladakh. This is parallel to 949
the mean present-day convergence orientation in this part of 950
the belt, as indicated, for instance, by earthquake focal 951
mechanisms. In the Kashmir syntaxis, where the density 952
of our measurements is much lower than in the north, we 953
find the same compressional stress field in the Miocene 954
Murree sandstones, folded in NNW–SSE striking isoclinal 955
folds (site 06-20, Figure 10). This orientation of the com- 956
pressional stress axis is in good accordance with the focal 957
mechanism of the 2005 Balakot earthquake that took place 958
in this area. The same compression orientation has been 959
recorded in the Pattan area (Besham syntaxis) by Zeilinger 960
et al. [2000], who also correlate it to the most recent 961
(Pleistocene) stress field. In this area as well, the inferred 962
recent stress field is in good accordance with focal mech- 963
anisms of the 1974 Pattan earthquake as well as aftershocks 964
of the 2005 Balakot earthquake. We have not found indi- 965
cations for this compression orientation in the central part of 966
Ladakh and Kohistan, which appear to react currently as 967
rigid blocks, with deformation mainly concentrated on their 968
borders. 969

[54] Compressional stress with a N–S to NN E–SSW 970
oriented σ_1 axis has been observed in some outcrops in the 971
Skardu area. The same σ_1 orientation is widely observed in 972

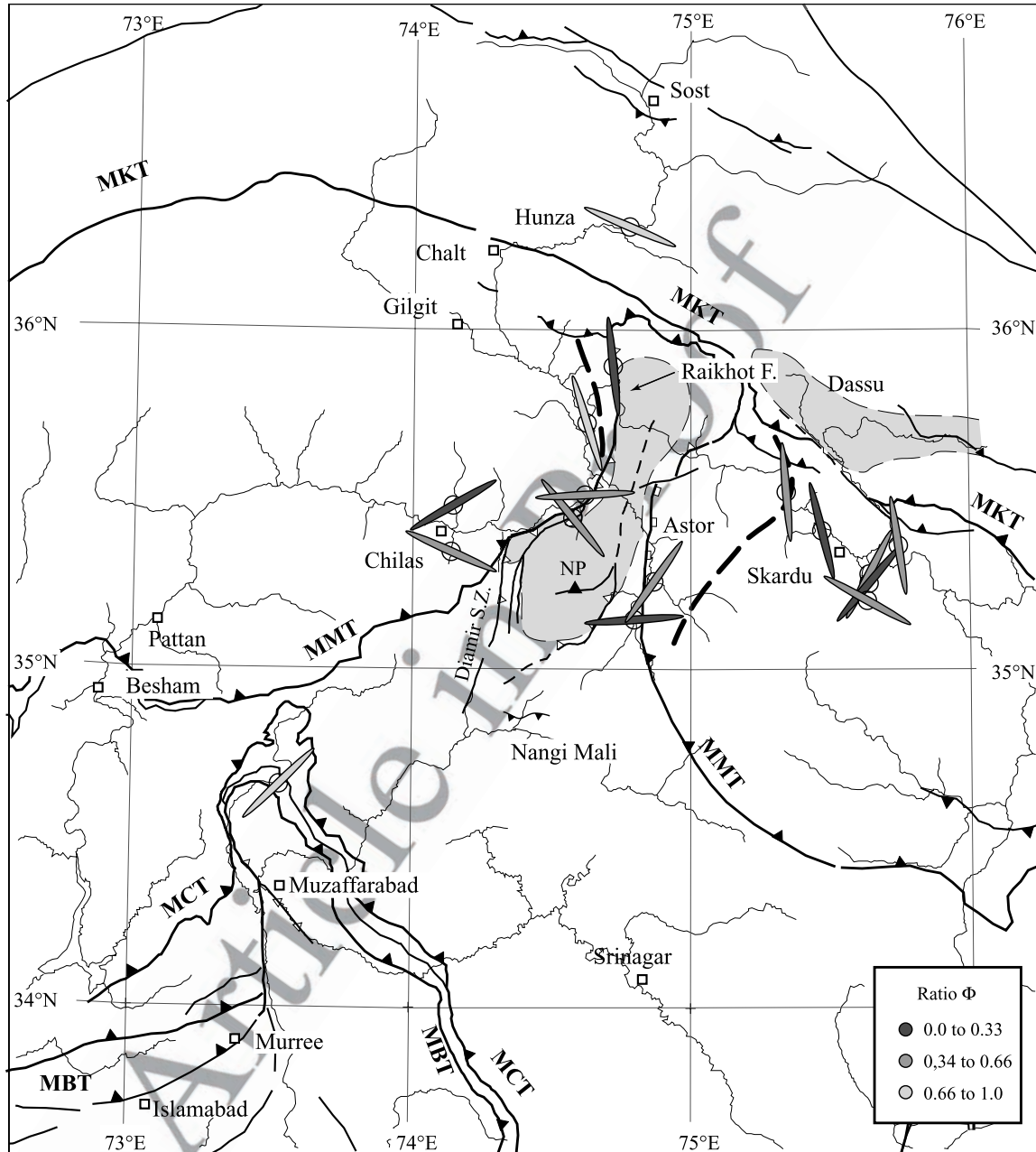


Figure 11a. Paleostress orientations from individual sites measurements. Compressional strain; σ_3 close to vertical (plunge $>70^\circ$), σ_1 and σ_2 horizontal (plunge $<20^\circ$) Grey ellipses indicate orientation of σ_1 .

973 Kohistan and Karakorum, but in a wrench tectonic context
 974 (see below). It is roughly parallel to the average Himalayan
 975 convergence orientation, but oblique with respect to modern
 976 convergence across the western Himalaya. The
 977 corresponding fault/striae couples could represent traces of
 978 brittle deformation dating from before the onset of Nanga
 979 Parbat exhumation (e.g., site 00-67, Figure 10, which
 980 feature a NNE–SSW compression prior to ENE–WSW
 981 compression), thus recording Miocene or older deformation.

5.2. Wrench-Type Stress Fields

[55] Figure 11b shows the σ_1 and σ_3 orientations for sites
 where both are close to horizontal. This situation corre-
 sponds to wrench-type strain, mainly marked by steeply
 dipping faults with low-pitch striae. We observe two of the
 main σ_1 orientations also observed in the compressional
 tensors; this parallelism suggests that the change from
 compression to wrenching corresponds to a permutation
 of the σ_2 and σ_3 axes in an unstable stress field.

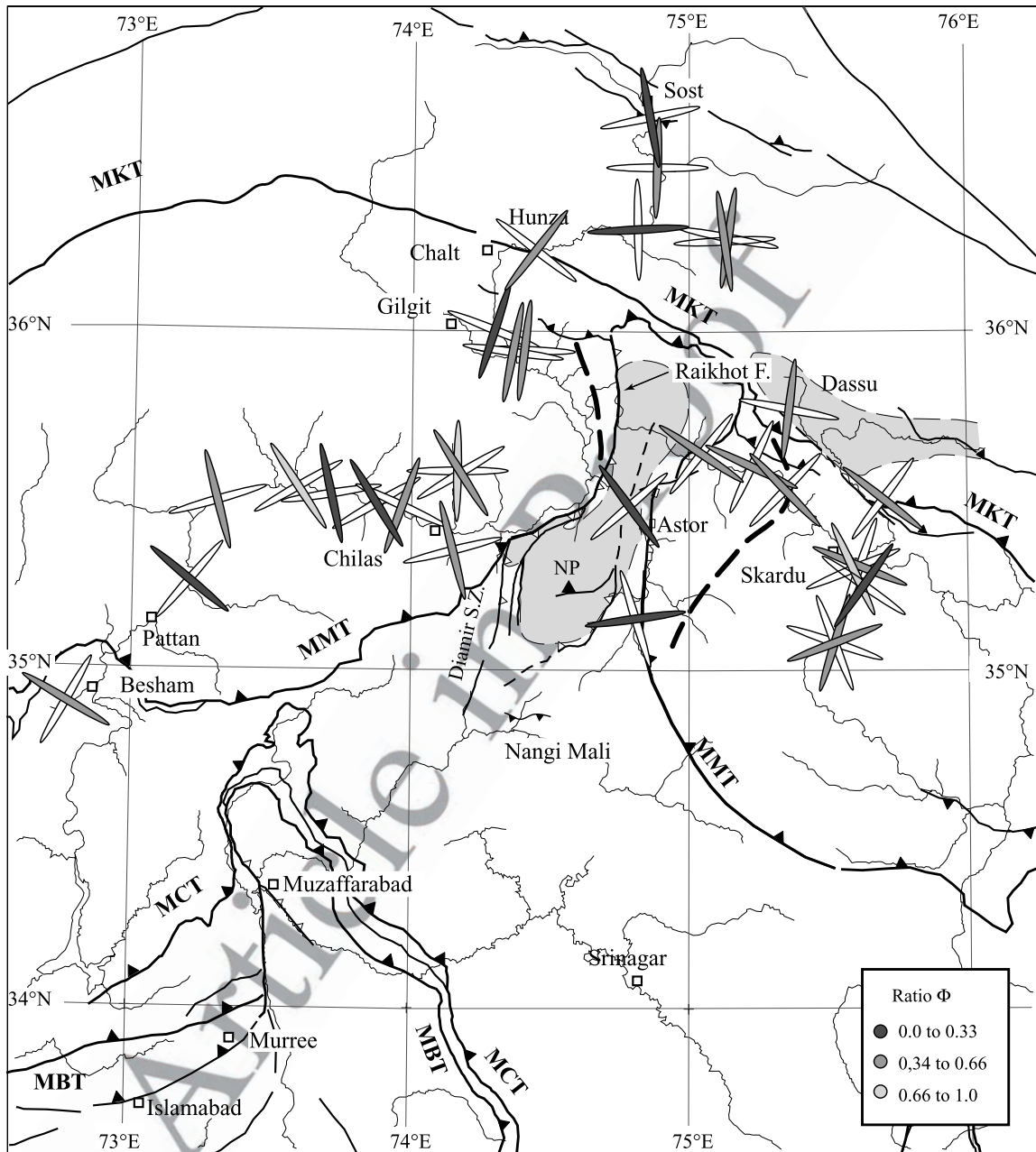


Figure 11b. Paleostress orientations from individual sites measurements. Wrench strain; σ_2 close to vertical (plunge $>70^\circ$), σ_1 and σ_3 close to horizontal (plunge $<20^\circ$). Grey ellipses indicate orientation of σ_1 . Plain ellipses: orientation of σ_3 .

991 [56] Compression parallel to the belt is widely encountered east of the Raikhot fault, but not west of it, in the
 992 Kohistan block. This pattern suggests that deformation in the Kohistan block was inhibited, most of the shortening
 993 parallel to the belt being absorbed in the hot and ductile Nanga Parbat pop-up structure. It thus confirms the importance of the Raikhot fault as a major structural boundary
 994 between a rigid and cold Kohistan block to the west and a locally reheated Ladakh block to the east.

[57] The same stress orientation as east of the Nanga 1000 Parbat is observed in the Besham syntaxis, both in the
 1001 hanging wall and footwall of the MMT. In this area, the tectonic pattern is similar to that encountered in Nanga
 1002 Parbat: the MMT is folded in a large N–S anticline and the
 1003 Himalayan series appear in the unroofed core of the
 1004 syntaxis. The Besham syntaxis could be a second zone
 1005 where shortening parallel to the belt is absorbed, but this
 1006 zone has either been aborted, or is currently at a less
 1007
 1008

1009 evolved stage than Nanga Parbat. In a previous study
 1010 limited to this zone, *Zeilinger et al.* [2000] depicted the
 1011 stress orientations using a direct inversion method (FSA
 1012 code [Célérier, 1995]). They also found an E–W orientation
 1013 for σ_1 and suggest, as we do, an early Pliocene age for this
 1014 tensor, associated with the onset of Nanga Parbat extrusion.
 1015 But instead of a wrench regime (σ_2 vertical), they found a
 1016 compressional regime (σ_3 vertical); it is difficult to say if
 1017 this discrepancy is due to different sampling of faults in the
 1018 field, to the different processing of the data, or if it reflects
 1019 some instability of the stress state. We favor the two last
 1020 hypotheses, as both *Zeilinger et al.* [2000] and ourselves
 1021 found tensors with low shape ratios Φ (close to 0). Such
 1022 tensors are characterized by similar magnitudes for σ_2 and
 1023 σ_3 , allowing easy permutation from compression to wrench
 1024 regimes. The difference may thus not be significant.

1025 [58] Wrench-type stress fields with a N–S oriented σ_1
 1026 axis were found in central Kohistan and in the Karakorum.
 1027 In northern Karakorum, our data are fully consistent with
 1028 the previous data of *Zanchi and Gritti* [1996] in Sost area,
 1029 acquired using the *Angelier* [1984] method. As previously
 1030 discussed, stress tensors with N–S oriented σ_1 axis could
 1031 correspond to a Miocene or earlier (pre-Nanga Parbat
 1032 anticline) regional stress field. We have not found evidence
 1033 for this stress tensor in the few sites that we have studied
 1034 along the Indus in the Besham syntaxis. It has been found,
 1035 however, by *Zeilinger et al.* [2000], who suggest a late
 1036 Miocene to Pliocene age for it.

1037 [59] The maps in Figures 10 and 11b suggest some
 1038 reorientation of the stress field close to the MKT, in the
 1039 Chalt-Gilgit area, where σ_1 appears to rotate to an orienta-
 1040 tion perpendicular to the MKT. Such rotation can be
 1041 interpreted as a block boundary effect, that is, local rotation
 1042 of the stress field against the Kohistan-Karakorum bound-
 1043 ary, a zone of transpression, as indicated by dextral strike-
 1044 slip displacement [*Coward et al.*, 1986]. It can also
 1045 indicate different predominant imprints of late Miocene
 1046 N–S shortening and modern NNE–SSW shortening per-
 1047 pendicular to the belt. Similarly, in central Kohistan the
 1048 dominant σ_1 orientation is not N–S, but NNW–SSE. In
 1049 this area, stress fields could have been partly controlled by
 1050 the local orientation of the MKT to the NW and the MMT
 1051 to the SE. However, our network of sites is not dense and
 1052 wide enough to determine whether these variations are
 1053 significant.

1054 5.3. Extensional Stress Fields

1055 [60] Figure 11c shows the sites for which a significant
 1056 part of the fault set is accounted for by a tensor with σ_1
 1057 close to vertical (plunge > 70°). Such a stress field corre-
 1058 sponds to extensional strain in the orientation of σ_3 . The
 1059 map underscores the widespread nature of extension, which
 1060 is concentrated in the zones of recent ductile exhumation,
 1061 but not restricted to those. The dominant σ_3 orientation is
 1062 roughly W–E, i.e., slightly oblate to the belt (transtension),
 1063 with not much change when moving from Karakorum to
 1064 Kohistan, or from Kohistan to Ladakh. Similar extension is
 1065 observed in the Nanga Parbat spur (Astor valley). This
 1066 extension is marked by faults with chlorite coating or by dry

1067 faults, formed during cooling of the Nanga Parbat gneiss.
 1068 Accordingly, it should be younger than 5 Ma, or even 2 Ma
 1069 (average Ar/Ar mica ages in the core of this zone). If we
 1070 assume that the W–E to WNW–ESE extension observed in
 1071 Karakorum and from Gilgit to Skardu has the same age, it
 1072 implies widespread post-5 Ma perpendicular to convergence
 1073 extension in this part of the belt. However, we also
 1074 recognize a N–S to NNW–SSE extension orientation in
 1075 Nanga Parbat as well as in the Dassu area. As noted
 1076 previously (compare Figure 9), this second orientation
 1077 appears to be predominant east of the Raikhot fault, in the
 1078 Nanga Parbat, Randu, and Braldu areas. Nevertheless, its
 1079 pattern varies from site to site.

1080 [61] In the central Nanga Parbat zone, ductile structures
 1081 are dominated by NNE–SSW striking isoclinal folds, and a
 1082 N–S stretching lineation, partly inherited from preceding
 1083 MMT thrusting. Some N–S ductile extension, corresponding
 1084 to normal-sense north oriented displacement, could have
 1085 occurred in the footwall of the Main Mantle Thrust, prior to
 1086 the Nanga Parbat fold formation [*Argles and Edwards*,
 1087 2002]. The N–S brittle extension observed in the same
 1088 zone could mark the continuation of this extension from
 1089 prior to 5 Ma (probable initiation of the Nanga Parbat fold)
 1090 until at least 2 Ma. NNW–SSE to NNE–SSW extension is
 1091 also observed in the Besham syntaxis [*Zeilinger et al.*,
 1092 2007], which we already argued to be a similar structure
 1093 to Nanga Parbat, and where the deep gorge of the Indus
 1094 River flowing down from central Kohistan may reflect
 1095 recent uplift.

1096 [62] North of Skardu, in the southern Karakorum, Plio-
 1097 cene exhumation of middle crust as in Nanga Parbat also
 1098 occurs in the core of dome-shaped folds. We have measured
 1099 fault sites only in the Dassu dome, the easternmost of a
 1100 series of E–W trending domes between the right-lateral
 1101 Shigar and Karakorum faults. If we consider the bulk set of
 1102 faults from the four sites located on the Dassu dome
 1103 (Braldu-Dassu area in Figure 8), the best defined tensors
 1104 are characterized by vertical σ_1 and N–S oriented σ_3 . In
 1105 more detail, the multiple inverse method analysis for this
 1106 area (Figure 12) shows a well-defined cluster for σ_1 ,
 1107 implying that the vertical orientation obtained for σ_1 is
 1108 robust. In contrast, σ_3 solutions are spread throughout the
 1109 horizontal plane, with Φ ratios around 0.3 to 0.5. This
 1110 pattern is characteristic of multidirectional extension, with
 1111 only a weak preference for N–S extension, and thus mimics
 1112 (and probably closely followed) ductile radial extension
 1113 observed in the same domes [*Mahéo et al.*, 2004].

1114 [63] At the northern termination of the Nanga Parbat
 1115 anticline, the ductile gneissic fabric draws two juxtaposed
 1116 domal structures, as indicated by the mapping of *Le Fort*
 1117 and *Pécher* [2002]. Fault sites located around the domes in
 1118 this area also indicate radial extension, mimicking the
 1119 earlier ductile extension marked by stretching lineations.

1120 [64] The coexistence of N–S extension in both the Dassu
 1121 dome and the Nanga Parbat and Besham syntaxes, which
 1122 display different regional structural orientations (N–S for
 1123 the Nanga Parbat and Besham syntaxis folds, E–W for the
 1124 Karakorum domes), indicates that such extension was not
 1125 only locally controlled by the geometry of the folds and

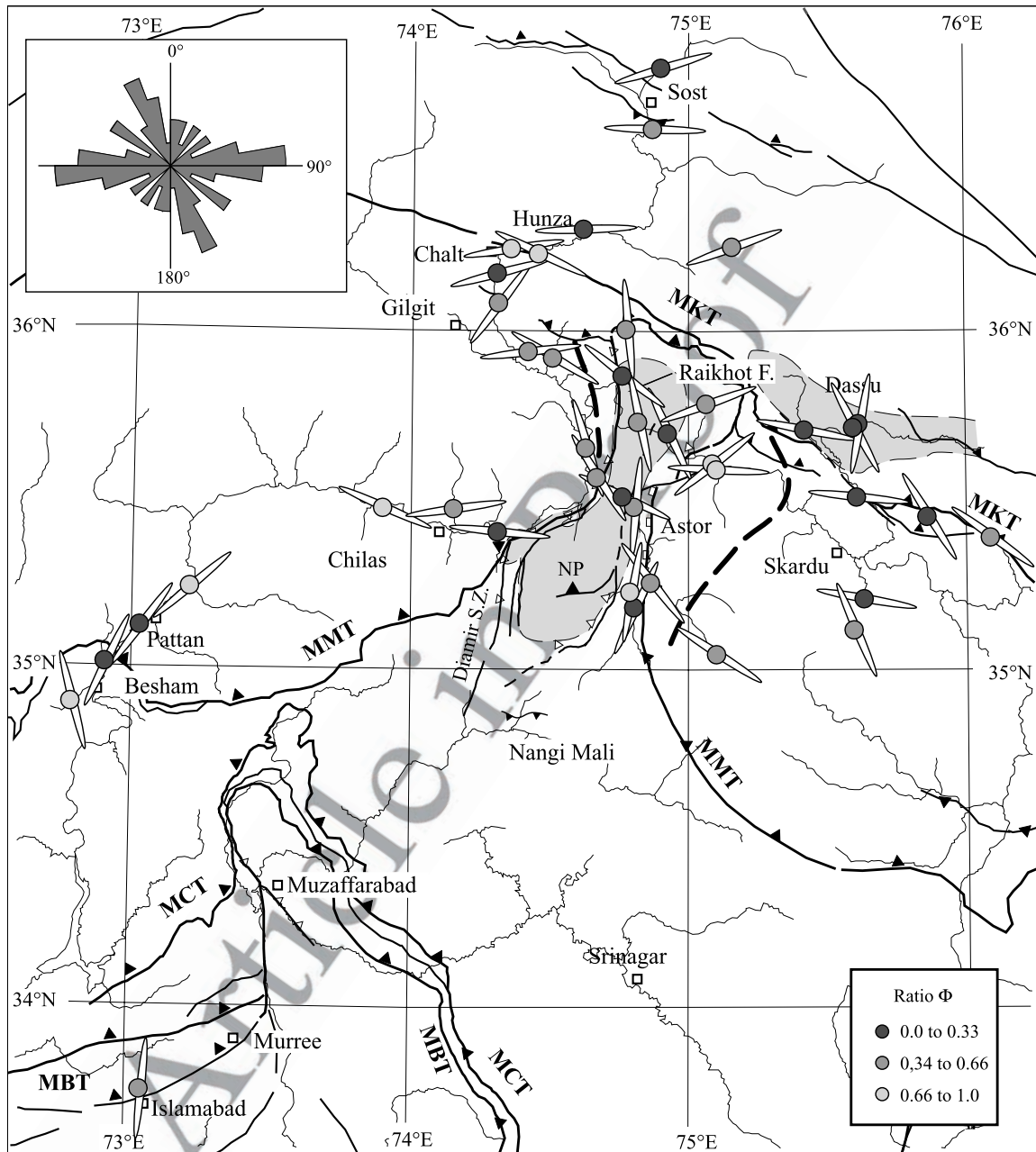


Figure 11c. Paleostress orientations from individual sites measurements. Extension strain; σ_1 close to vertical (plunge $>70^\circ$), σ_2 and σ_3 horizontal (plunge $<20^\circ$) Plain ellipses indicate orientation of σ_3 . The rose diagram shows the orientations of σ_3 (39 values, classes of 10° , maximum 6 values).

1126 domes, but implies spreading of the crust at a larger scale
 1127 (hundreds of kilometers). The same is true for E–W
 1128 extension, which is observed in the Karakorum, northern
 1129 Kohistan, and Ladakh. It is difficult to establish a relative
 1130 chronology for these two regional Plio-Pleistocene exten-
 1131 sion orientations. Radial to N–S extension is common to
 1132 both ductile and brittle regimes. We suggest that this brittle
 1133 deformation is a continuation of the similarly oriented
 1134 ductile deformation and would thus be older than WNW–

ESE extension. This brittle extension is uncorrelated with
 the ductile strain pattern and may thus postdate Nanga
 Parbat doming. Actually, it corresponds to the present-day
 extension in this area, as indicated by the focal mechanism
 solutions.

5.4. Tilted Tensors

[65] Altogether, about one third of the calculated tensors
 have principal axes that are significantly tilted (more than

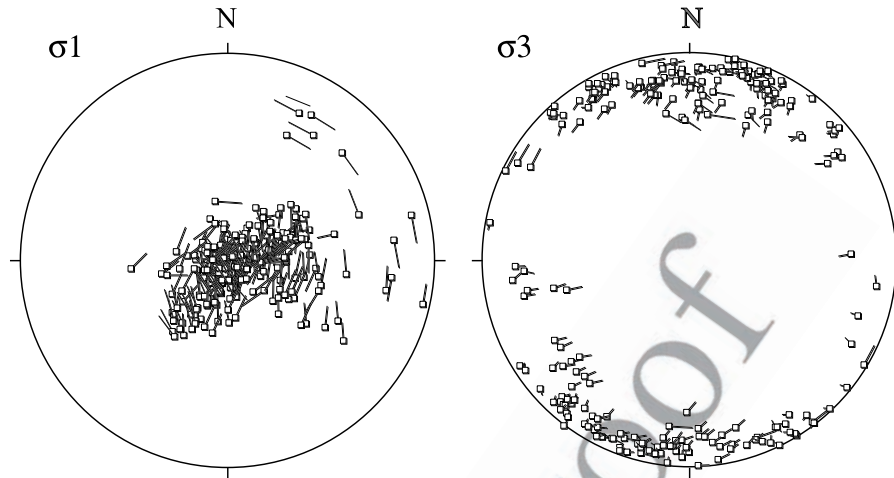


Figure 12. Dassu-Braldu area, results from the multiple inverse methods (software package mim5-miv4, A. Yamaji et al., Multiple Inverse Method Software Package, Freeware package, 2005, <http://www.kueps.kyoto-u.ac.jp/~yamaji/PDS/indexe.html>); 235 points (from a 60 000 nods grid) having a significant number of solutions tied to them [see Yamaji et al., 2005], plotted in lower hemisphere, equal-area projections. (left) stereogram for σ_1 , clustered close to vertical. (right) Stereogram for σ_3 , with a poorly defined NNE-SSW best position.

1143 20°) with respect to the vertical or horizontal. These tensors
 1144 are indicated on Figure 10 where the tilt of the principal axis
 1145 is indicated by the degree of ellipticity of the symbol. They
 1146 do not fit the widely accepted Andersonian faulting theory,
 1147 which states that near the free surface, where shear stress is
 1148 nil, one of the principal stress axes is normal to the surface
 1149 and others two are parallel to it. In low-relief areas, these
 1150 orientations are nearly vertical and horizontal, but in the
 1151 high relief of the study region stress axes that obey
 1152 Andersonian theory can be significantly oblique. The tilted
 1153 tensors can thus be due to either local perturbations of the
 1154 stress field by topography, or to passive postfaulting rotation
 1155 of the set of faults on which the tensor was calculated.

1156 [66] In northern Pakistan, the thermal gradient is particu-
 1157 larly high in the rapidly exhuming areas (Nanga Parbat,
 1158 eastern Karakorum), and lifts the brittle-ductile transition up
 1159 to a few km below the surface. The brittle-ductile transition
 1160 has been located from microseismicity at only 5–6 km
 1161 depth below Nanga Parbat [Meltzer et al., 2001] while
 1162 topography over a distance of only 15 km ranges between
 1163 8 km at the summit of Nanga Parbat to 1 km along the Indus
 1164 River. Topographic stresses can thus be expected to have a
 1165 significant effect over the entire brittle crust.

1166 [67] In effect, tilted tensors are mainly observed in the
 1167 broad Nanga Parbat zone as previously defined (i.e., the
 1168 Nanga Parbat spur and adjacent western Ladakh).
 1169 The Nanga Parbat has evolved during the Pliocene as a
 1170 pop-up anticline, extruded between two N–S ductile shear
 1171 zones [Schneider et al., 1999; Edwards et al., 2000]: the
 1172 Diamir shear zone, which is the southern prolongation of
 1173 the Quaternary Raikhot fault to the west and the Rupal shear
 1174 zone to the east (Figure 1). Recent exhumation of Nanga
 1175 Parbat is concentrated in the core of the N–S anticline, at a

rate of 5–10 mm a⁻¹ [Zeitler et al., 1993; Schneider et al.,
 1999; Zeitler et al., 2001a]. In many sites of this area, σ_3
 remains roughly horizontal and parallel to the fold axis; σ_1
 axis is not tilted around an axis parallel to the river gorges,
 as would be expected for topographic effects, but remains
 perpendicular to the fold, with various plunges (from
 horizontal to vertical). Thus in Nanga Parbat, tilted tensors
 can be most easily explained by passive rotation of the
 faults around the N–S axis of the growing pop-up anticline
 rather than by topographic effects.

6. Conclusions

[68] The aim of this study is to provide a comprehensive
 overview of the paleostress patterns in northern Pakistan.
 We have underlined the challenges associated with fault
 inversion studies in an area of multistage and heterogeneous
 deformation. The tasks include recognizing the superim-
 posed tensors and establishing their chronology, using
 intrinsic information from the sites themselves.

[69] In a heterogeneous stress field, results could be
 sampling-dependent because the imprint of the different
 stress events is not the same at different sites. This could
 especially be a problem in zones of low-density sampling of
 faults. Results could also be partly method-dependent. For
 the southern part of our study area, we have been able to
 compare our results with those of two previous studies that
 employed a different inversion method [Zeilinger et al.,
 2000; Burg et al., 2005b]. At a regional scale, we obtained a
 similar superposition of stress regimes, i.e., successively
 NNE–SSW compression (in a compression or wrench
 strain regime), E–W compression, extension (E–W and
 radial instead of NW–SE), and finally NE–SW to NNE–

1208 SSW compression (compatible with the Balakot earth-
1209 quake). At a more local scale (for instance, along the Indus
1210 section in the Besham syntaxis), however, we notice some
1211 discrepancies such as different relative imprints of the
1212 successive tensors, slight orientation discrepancies, larger
1213 discrepancies in the Φ ratio and, associated with the latter,
1214 possible permutation of the σ_1 – σ_2 or σ_2 – σ_3 axes.

1215 [70] The relative chronology and time bracketing of
1216 successive stress fields has been mainly based on regional
1217 continuity and comparison with better dated ductile tecton-
1218 ics. This proved a relatively easy task north of the MMT and
1219 in the Nanga Parbat area, where the density of measurement
1220 sites was sufficiently high to verify the coherence of the
1221 results from one site to another and to evidence regional
1222 trends. It was less successful in the Kashmir syntaxis to the
1223 south of Nanga Parbat where faults sites were scarcer, partly
1224 due to lack of propitious outcrops and partly due to access
1225 restrictions. Despite these limits, the applied method evi-
1226 dences a recent (mainly Pliocene and Pleistocene) paleo-
1227 stress pattern in northern Pakistan, which is well reflected
1228 by the main geomorphologic units.

1229 [71] The oldest recorded stress field predates Pliocene-
1230 Quaternary exhumation of Nanga Parbat and Karakorum. It
1231 corresponds to NNE–SSW shortening in a wrench strain
1232 regime, in response to Indian-Asian convergence. The σ_1
1233 principal stress axis is roughly N–S, while σ_3 is E–W. Its
1234 imprint is mainly preserved in Kohistan and Deosai, which
1235 were probably tectonically and morphologically stabilized
1236 as early as middle Miocene. It is also observed in the central
1237 Karakorum, however, which remained thermally active until
1238 at least the Upper Miocene, as indicated by emplacement of
1239 Sumayar leucogranite (Hunza area) at 9.2 Ma [Fraser *et al.*,
1240 1999]. In the Karakorum, this initial stress field is coherent
1241 with the late nappe stacking to the south.

1242 [72] The Mio-Pliocene initiation of the Nanga Parbat
1243 system of N–S trending folds marks the appearance of a
1244 new regional stress state, which also corresponds to wrench-
1245 ing, but with shortening oriented parallel to the belt (σ_1
1246 WNW–ESE, and σ_3 SSW–NNE). The Nanga Parbat
1247 appears as a tectonic singularity, where most of the short-
1248 ening is absorbed and the excess crustal volume eroded. Its
1249 western limit is the Raikhot fault: the imprint of the stress
1250 field characterized by E–W compression is clear to the east
1251 of this fault, in Ladakh and in the Nanga Parbat, but
1252 vanishes to the west of it. The Raikhot fault and its
1253 southward prolongation (the Diamir shear zone) act as a
1254 major N–S discontinuity, possibly inherited from a pre-
1255 Himalayan limit between two crustal segments of the crust
1256 with different bulk rheology within the Indian craton. The
1257 other main discontinuity is the vertical Shyok fault zone,
1258 which reactivates the Shyok suture zone and acts as a right-
1259 lateral transfer zone required to accommodate Nanga Parbat
1260 shortening. To the southwest of Nanga Parbat, the same
1261 paleostress orientation has been encountered in the Besham
1262 syntaxis, which could represent an aborted or immature
1263 structure similar to the Nanga Parbat pop-up.

[73] Plio-Pleistocene extension appears as an outstanding
1264 feature. It is predominantly multidirectional. Nevertheless,
1265 there seems to be a transition in time from a N–S to an E–
1266 W orientation of the main extension orientation. Strong
1267 exhumation of Nanga Parbat, lateral collapse of the hanging
1268 wall of the Nanga Parbat fold and final extrusion of the
1269 Dassu dome, are all associated with vertical σ_1 , and
1270 occurred during this extensional phase. This extension is
1271 not restricted to the zones of rapid exhumation, however,
1272 but appears widespread across northern Pakistan. This phase
1273 can possibly be linked to widespread E–W extension that
1274 affected the Tibetan Plateau farther east during the same
1275 period [Armijo *et al.*, 1986].
1276

[74] Finally, we have observed NE–SW compression in
1277 Ladakh and in the northern part of the Kashmir syntaxis.
1278 This stress field is characterized by a σ_1 axis perpendicular
1279 to the strike of the belt and parallel to present-day com-
1280 pression, as evidenced by earthquake focal mechanisms, in
1281 particular those of the 1974 Pattan and 2005 Balakot
1282 earthquakes.
1283

[75] The timing of the first and last stages is best con-
1284 strained. The relation between the stage(s) of compression
1285 parallel to the belt and the stage(s) of extension is more
1286 ambiguous. We propose a Mio-Pliocene age for shortening
1287 parallel to the belt, based on the age of the onset of N–S
1288 fold axis in Nanga Parbat. Along-strike compression is
1289 consistent with the Seeber and Pêcher [1998] model of
1290 strain partitioning along the Himalayan arc and the Nanga
1291 Parbat antiform. However, this model is based on the
1292 present-day geometry of the Himalayan arc and radial
1293 convergence, and we cannot be certain it applies for the
1294 Pliocene period. Moreover, the distribution of focused low-
1295 velocity anomalies below the Nanga Parbat inferred from
1296 geophysical data [Zeitler *et al.*, 2001a, and references
1297 therein] suggests rapid exhumation of rocks from midcrustal
1298 depths, which fits better with extension and a vertical σ_1 , as
1299 observed in the fault data and in seismicity (Figure 2),
1300 which indicates today ENE–WSW extension in Nanga
1301 Parbat.
1302

[76] Regardless of the chronology at a million year scale
1303 of shortening parallel to the belt, extension parallel to the
1304 belt and vertical extrusion, the N–W Himalayan syntaxis is
1305 clearly a zone of tectonic and stress instability during its
1306 entire Pliocene-Quaternary history. Multidirectional exten-
1307 sion is juxtaposed on short time periods to shortening either
1308 parallel or perpendicular to the belt. These differences may
1309 stem from stress axes permutations rather than changes in
1310 orientation. Such coexistence or juxtaposition could be
1311 typical of strain and stress partitioning during oblique
1312 convergence.
1313

[77] **Acknowledgments.** This work summarizes data collected during
1314 many campaigns of field work in northern Pakistan and has benefited
1315 during the last years from the support of the Geological Survey of Pakistan,
1316 the French Embassy in Islamabad, and the ANR program PAKSIS. We
1317 thank two referees for their constructive and very detailed reviews.
1318

References

- Angelier, J. (1975), Sur l'analyse des mesures recueillies dans des sites failles: L'utilité d'une confrontation entre les méthodes dynamiques et cinématiques, *C. R. Acad. Sci.*, **281**, 1805–1808.
- Angelier, J. (1979), Determination of the mean principal directions of stresses for a given fault population, *Tectonophysics*, **56**, T17–T26, doi:10.1016/0040-1951(79)90081-7.
- Angelier, J. (1984), Tectonic analysis of fault slip data sets, *J. Geophys. Res.*, **89**, 5835–5848, doi:10.1029/JB089iB07p05835.
- Argles, T. W., and M. A. Edwards (2002), First evidence for high-grade, Himalayan-age synconvergent extension recognised within the western syntaxis—Nanga Parbat, Pakistan, *J. Struct. Geol.*, **24**, 1327–1344, doi:10.1016/S0191-8141(01)00136-5.
- Armijo, R., E. Carey, and A. Cisternas (1982), The inverse problem in microtectonics and the separation of tectonic phases, *Tectonophysics*, **82**, 145–160, doi:10.1016/0040-1951(82)90092-0.
- Armijo, R., P. Tapponnier, J. L. Mercier, and H. Tong-Li (1986), Quaternary extension in southern Tibet: Field observations and tectonic implications, *J. Geophys. Res.*, **91**, 13,803–13,872, doi:10.1029/JB091iB14p13803.
- Armijo, R., P. Tapponnier, and H. Tonglin (1989), Late Cenozoic right-lateral strike-slip faulting in southern Tibet, *J. Geophys. Res.*, **94**, 2877–2838, doi:10.1029/JB094iB03p02787.
- Avouac, J. P., and P. Tapponnier (1993), Kinematic model of active deformation in central Asia, *Geophys. Res. Lett.*, **20**(10), 895–898, doi:10.1029/93GL00128.
- Bendick, R., and R. Bilham (2001), How perfect is the Himalayan arc?, *Geology*, **29**, 791–794, doi:10.1130/0091-7613(2001)029<0791:HPITHA>2.0.CO;2.
- Bertrand, J., J. Kienast, and J. Pinardon (1988), Structure and metamorphism of the Karakoram gneisses in the Braldu-Baltoro valley (north Pakistan), *Geodin. Acta*, **2**, 135–150.
- Bishop, A. W. (1966), The strength of solids as engineering materials, *Geotechnique*, **16**, 91–130.
- Bossart, P., and R. Ottiger (1989), Rocks of the Murree Formation in Northern Pakistan: Indicators of a descending foreland basin of late Palaeocene to middle Eocene age, *Eclogae Geol. Helv.*, **82**, 133–165.
- Bott, M. H. P. (1959), The mechanics of oblique slip faulting, *Geol. Mag.*, **96**, 109–117.
- Brandon, M. T., M. Roden-Tice, and J. I. Garver (1998), Late Cenozoic exhumation of the Cascadia accretionary wedge in the Olympic Mountains, northwest Washington State, *Geol. Soc. Am. Bull.*, **110**, 985–1009, doi:10.1130/0016-7606(1998)110<0985:LCEOTC>2.3.CO;2.
- Burbank, D. W., R. G. H. Reynolds, and G. H. Johnson (1986), Late Cenozoic tectonics and sedimentation in the north-western Himalayan foredeep: II. Eastern limb of the northwest syntaxis and regional synthesis, *Spec. Publ. Int. Assoc. Sedimentol.*, **8**, 293–306.
- Burbank, D. W., J. Leland, E. Fielding, R. S. Anderson, N. Brozovic, M. R. Reid, and C. Duncan (1996), Bedrock incision, rock uplift and threshold hillslopes in the northwestern Himalayas, *Nature*, **379**, 505–510, doi:10.1038/379505a0.
- Burg, J. P., P. Nievergelt, F. Oberli, D. Seward, P. Davy, J. C. Maurin, Z. Diao, and M. Meier (1998), The Namche Barwa syntaxis: Evidence for exhumation related to compressional crustal folding, *J. Asian Earth Sci.*, **16**(2–3), 239–252, doi:10.1016/S0743-9547(98)00002-6.
- Burg, J. P., L. Arbaret, N. M. Chaudhry, H. Dawood, S. Hussain, and G. Zeilinger (2005a), Shear strain localization from the upper mantle to the middle crust of the Kohistan Arc (Pakistan), in *Fluid Motions in Volcanic Conduits: A Source of Seismic and Acoustic Signals*, edited by S. J. Lane and J. S. Gilbert, *Geol. Soc. Spec. Publ.*, **245**, 25–38, doi:10.1144/GSL.SP.2005.245.01.02.
- Burg, J. P., B. Célérier, N. M. Chaudhry, M. Ghazanfar, F. Gnehm, and M. Schnellmann (2005b), Fault analysis and paleostress evolution in large strain regions: Methodological and geological discussion of the southeastern Himalayan fold-and-thrust belt in Pakistan, *J. Asian Earth Sci.*, **24**, 445–467, doi:10.1016/j.jseas.2003.12.008.
- Butler, R. W. H., and D. J. Prior (1988), Tectonic controls on the uplift of the Nanga Parbat Massif, Pakistan Himalayas, *Nature*, **333**, 247–250, doi:10.1038/333247a0.
- Célérier, B. (1995), Tectonic regime and slip orientation of reactivated faults, *Geophys. J. Int.*, **121**, 143–161, doi:10.1111/j.1365-246X.1995.tb03517.x.
- Coward, M. P., D. C. Rex, M. Asif Khan, B. F. Windley, R. D. Broughton, I. W. Luff, M. G. Pettersen, and C. J. Pudsey (1986), Collision tectonics in the NW Himalayas, in *Collision Tectonics*, edited by M. P. Coward and A. C. Reis, *Geol. Soc. Spec. Publ.*, **19**, 203–219.
- Coward, M. P., R. W. H. Butler, M. Asif Khan, and R. J. Knipe (1987), The tectonic history of Kohistan and its implication for Himalayan structure, *J. Geol. Soc.*, **144**(3), 377–391, doi:10.1144/gsjgs.144.3.0377.
- DeCelles, P. G., D. M. Robinson, and G. Zandt (2002), Implications of shortening in the Himalayan fold-thrust belt for uplift of the Tibetan Plateau, *Tectonics*, **21**(6), 1062, doi:10.1029/2001TC001322.
- DiPietro, J. A., and K. R. Pogue (2004), Tectonostratigraphic subdivisions of the Himalaya: A view from the west, *Tectonics*, **23**, TC5001, doi:10.1029/2003TC001554.
- DiPietro, J. A., A. Hussain, I. Ahmad, and M. A. Khan (2000), The main mantle thrust in Pakistan: Its character and extent, in *Tectonics of the Nanga Parbat Syntaxis and the Western Himalaya*, edited by M. A. Khan et al., *Geol. Soc. Spec. Publ.*, **170**, 375–393.
- Edwards, M. A., W. S. Kidd, M. A. Khan, and D. A. Schneider (2000), Tectonics of the SW margin of the Nanga Parbat-Haramosh massif, in *Tectonics of the Nanga Parbat Syntaxis and the Western Himalaya*, edited by M. A. Khan et al., *Geol. Soc. Spec. Publ.*, **170**, 77–100.
- Etchecopar, A., G. Vasseur, and M. Daignières (1981), An inverse problem in microtectonics for the determination of stress tensors from fault striation analysis, *J. Struct. Geol.*, **3**, 51–65, doi:10.1016/0191-8141(81)90056-0.
- Fontan, D., M. Schoupe, C. J. Hunziker, G. Martinotti, and J. Verpkaeren (2000), Metamorphic evolution, ⁴⁰Ar–³⁹Ar chronology and tectonic model for the Neelum valley, Azad Kashmir, NE Pakistan, in *Tectonics of the Nanga Parbat Syntaxis and the Western Himalaya*, edited by A. Khan et al., *Geol. Soc. Spec. Publ.*, **170**, 431–453.
- Fraser, J. E., M. P. Searle, R. R. Parrish, and S. R. Noble (1999), U–Pb geochronology on the timing of metamorphism and magmatism in the Hunza Karakorum (abstract), *Terra Nostra*, **99**(2), 45–46.
- Fraser, J. E., M. P. Searle, R. R. Parrish, and S. R. Noble (2001), Chronology of deformation, metamorphism and magmatism in southern Karakoram Mountains, *Geol. Soc. Am. Bull.*, **113**, 1443–1455, doi:10.1130/0016-7606(2001)113<1443:CODMAM>2.0.CO;2.
- Gaetani, M. (1997), The Karakorum Block in central Asia, from Ordovician to Cretaceous, *Sediment. Geol.*, **109**, 339–359, doi:10.1016/S0037-0738(96)00068-1.
- Greco, A. (1991), Tectonics and metamorphism in the western Himalayan syntaxis area (Azad Kashmir, NE-Pakistan), *Mitt. Geol. Inst. Zurich*, **274**, 193 pp.
- Greco, A., G. Martinotti, K. Papritz, J. G. Ramsay, and R. Rey (1989), The crystalline rocks of the Kaghan valley (NE-Pakistan), *Eclogae Geol. Helv.*, **82**(2), 629–653.
- Grove, M., and T. M. Harrison (1996), ⁴⁰Ar diffusion in Fe-rich biotite, *Am. Mineral.*, **81**, 940–951.
- Guillot, S., G. Garzanti, D. Baratoux, D. Marquer, G. Maheo, and J. de Sigoyer (2003), Reconstructing the total shortening history of the NW Himalaya, *Geochem. Geophys. Geosyst.*, **4**(7), 1064, doi:10.1029/2002GC000484.
- Harrison, T. M., I. Duncan, and I. McDougall (1985), Diffusion of ⁴⁰Ar in biotite: Temperature, pressure, and compositional effects, (1985), *Geochim. Cosmochim. Acta*, **49**(11), 2461–2468, doi:10.1016/0016-7037(85)90246-7.
- Jouanne, F., J. L. Mugnier, J. F. Gamond, P. Le Fort, M. R. Pandey, L. Bollinger, M. Flouzat, and J. P. Avouac (2004), Current shortening across the Himalayas of Nepal, *Geophys. J. Int.*, **157**, 1–14, doi:10.1111/j.1365-246X.2004.02180.x.
- Kasmi, A. H., and Q. Jan (1997), *Geology and Tectonics of Pakistan*, 554 pp., Graphic Publ., Karachi, Pakistan.
- Krol, M. A., P. K. Zeitler, G. Poupeau, and A. Pecher (1996), Temporal variations in the cooling and denudation history of the Hunza plutonic complex, Karakoram Batholith, revealed by ⁴⁰Ar/³⁹Ar thermochronology, *Tectonics*, **15**(2), 403–415, doi:10.1029/95TC02424.
- Larson, K. M., R. Bürgmann, R. Bilham, and J. T. Freymueller (1999), Kinematics of the India-Eurasia collision zone from GPS measurements, *J. Geophys. Res.*, **104**, 1077–1093, doi:10.1029/1998JB900043.
- Le Fort, P., and A. Pêcher (2002), An introduction to the geological map of the area between Hunza and Baltistan, Karakoram-Kohistan-Ladakh-Himalaya region, northern Pakistan, scale 1:150,000, *Geologica*, **6**, 1–199.
- Leland, J., M. R. Reid, D. Burbank, R. Finkel, and M. Caffee (1998), Incision and differential bedrock uplift along the Indus River near Nanga Parbat, Pakistan Himalaya, from ¹⁰Be and ²⁶Al exposure age dating of bedrock straths, *Earth Planet. Sci. Lett.*, **154**, 93–107, doi:10.1016/S0012-821X(97)00171-4.
- Liesa, C., and R. J. Lisle (2004), Reliability of methods to separate stress tensors from heterogeneous fault-slip data, *J. Struct. Geol.*, **26**, 559–572, doi:10.1016/j.jsg.2003.08.010.
- Lode, W. (1925), Versuche über den Einfluss der mittleren Hauptspannung auf die Fließgrenze, *Z. Angew. Math. Mech.*, **5**, 142–144.
- Lombardo, B., and F. Rollo (2000), Two contrasting eclogite types in the Himalayas: Implications for the Himalayan orogeny, *J. Geodyn.*, **30**, 37–60, doi:10.1016/S0264-3707(99)00026-5.
- MacDougall, I., and T. M. Harrison (1999), *Geochronology and Thermochronology by the ⁴⁰Ar/³⁹Ar Method*, 2nd ed., 269 pp., Oxford Univ. Press, New York.
- Mahéo, G., A. Pêcher, S. Guillot, Y. Rolland, and C. Delacourt (2004), Exhumation of Neogene gneiss domes between oblique crustal boundaries in south Karakorum (northwest Himalaya, Pakistan), in *Gneiss Domes in Orogeny*, edited by D. L. Whitney, C. Teyssier, and C. S. Siddoway, *Spec. Pap. Geol. Soc. Am.*, **380**, 141–154.
- Meltzer, A., G. Sarker, B. Beaudoin, L. Seeber, and J. Armbruster (2001), Seismic characterization of an active metamorphic massif, Nanga Parbat, Pakistan, *Himalayan Geol.*, **29**, 651–654, doi:10.1130/0091-7613(2001)029<0651:SCOAAM>2.0.CO;2.
- Nemcek, M., and R. J. Lisle (1995), A stress inversion procedure for polyphase fault/slip data sets, *J. Struct. Geol.*, **17**(10), 1445–1453, doi:10.1016/0191-8141(95)00040-K.
- Otsubo, M., K. Sato, and A. Yamaji (2006), Computerized identification of stress tensor determined from heterogeneous fault-slip data by combining the multiple inverse method and k-means clustering, *J. Struct. Geol.*, **28**, 991–997, doi:10.1016/j.jsg.2006.03.008.
- Parrish, R. P., and R. Tirrul (1989), U–Pb ages of the Baltoro granite, northwest Himalaya, and implica-

- tions for monazite U-Pb systematics, *Geology*, 17, 1076–1079, doi:10.1130/0091-7613(1989)017<1076:UPAOTB>2.3.CO;2.
- Paul, J., et al. (2001), The motion and active deformation of India, *Geophys. Res. Lett.*, 28, 647–650, doi:10.1029/2000GL011832.
- Pêcher, A., and P. Le Fort (1999), Late Miocene tectonic evolution of the Karakoram-Nanga Parbat contact zone (northern Pakistan), in *Himalaya and Tibet: Mountain Roots to Mountain Tops*, edited by A. MacFarlane, J. Quade, and R. Sorkhabi, *Spec. Pap. Geol. Soc. Am.*, 328, 145–158.
- Pêcher, A., and L. Seeber (2003), Recent stress field in Nanga Parbat and southern Karakoram from faults inversion, paper presented at the 18th Himalaya-Karakoram-Tibet Workshop, ETH-Zurich, Ascona, Switzerland.
- Pêcher, A., G. Giuliani, A. B. Kausar, R. M. Malik, and H. R. Muntaz (2002), Geology and geochemistry of the Nangimali ruby deposit area, Nanga-Parbat Himalaya (Azra Kashmir, Pakistan), *J. Asian Earth Sci.*, 21(3), 265–282, doi:10.1016/S1367-9120(02)00041-X.
- Poupeau, G., A. Pêcher, M. Benharbit, and O. F. Noyan (1991), Ages traces de fission sur apatites et taux de dénaturation Plio-Quaternaires au Karakoram central, *C. R. Acad. Sci.*, 313, 917–922.
- Reuber, I. (1989), The Dras arc: Two successive volcanic events on eroded oceanic crust, *Tectonophysics*, 161, 93–106, doi:10.1016/0040-1951(89)90305-3.
- Robertson, A. H. F., and A. S. Collins (2002), Shyok Suture Zone, N Pakistan: Late Mesozoic-Tertiary evolution of a critical suture separating the oceanic Ladakh Arc from the Asian continental margin, *J. Asian Earth Sci.*, 20, 309–351, doi:10.1016/S1367-9120(01)00041-4.
- Rolland, Y., E. Carrio-Schaffhauser, S. M. F. Sheppard, A. Pêcher, and L. Esclauze (2006), Metamorphic zoning and geodynamic evolution of an inverted crustal section (Karakoram margin, N Pakistan), evidence for two metamorphic events, *Int. J. Earth Sci.*, 95, 288–305, doi:10.1007/s00531-005-0026-x.
- Rolland, Y., G. Mahéo, S. Guillot, and A. Pêcher (2001), Tectono-metamorphic evolution of the Karakoram Metamorphic Complex (Dassu-Askole area, NE Pakistan): Mid-crustal granulite exhumation in a compressive context, *J. Metamorph. Geol.*, 19, 717–737.
- Rolland, Y., A. Pêcher, and C. Picard (2000), Middle Cretaceous back-arc formation and arc evolution along the Asian margin: The Shyok Suture Zone in northern Ladakh (NW Himalaya), *Tectonophysics*, 325, 145–173, doi:10.1016/S0040-1951(00)00135-9.
- Rolland, Y., C. Picard, A. Pêcher, E. Carrio, S. M. F. Sheppard, S. M. Oddone, and I. Villa (2002), Presence and geodynamic significance of Cambro-Ordovician series of SE Karakoram (N Pakistan), *Geodin. Acta*, 15, 1–21, doi:10.1016/S0985-3111(01)01075-0.
- Schneider, D. A., M. A. Edwards, W. S. F. Kidd, M. Asif Khan, L. Seeber, and P. K. Zeitler (1999), Tectonics of Nanga Parbat, western Himalaya: Synkinematic plutonism within the doubly vergent shear zones of a crustal-scale pop-up structure, *Geology*, 27, 999–1002, doi:10.1130/0091-7613(1999)027<0999:TONPWH>2.3.CO;2.
- Schneider, D. A., P. K. Zeitler, W. S. F. Kidd, and M. A. Edwards (2001), Geochronologic constraints on the tectonic evolution and exhumation of Nanga Parbat, western Himalaya syntaxis, revisited, *J. Geol.*, 109, 563–583, doi:10.1086/322764.
- Scholz, C. H. (1988), The brittle-plastic transition and the depth of seismic faulting, *Geol. Rundsch.*, 77, 319–328, doi:10.1007/BF01848693.
- Scholz, C. H. (2002), *The Mechanics of Earthquakes and Faulting*, Cambridge Univ. Press, Cambridge, U.K.
- Searle, M. P., M. A. Khan, J. E. Fraser, S. J. Gough, and M. Q. Jan (1999), The tectonic evolution of the Kohistan-Karakoram collision belt along the Karakoram Highway transect, north Pakistan, *Tectonics*, 18(6), 929–949, doi:10.1029/1999TC900042.
- Searle, M. P., A. J. Rex, R. Tirrul, D. C. Rex, A. Barnicoat, and B. F. Windley (1989), Metamorphic, magmatic and tectonic evolution of the Central Karakoram in the Biafo-Baltoro-Hushe regions of northern Pakistan, in *Tectonics of the Western Himalayas*, edited by L. L. Malinconico, *Spec. Pap. Geol. Soc. Am.*, 232, 47–73.
- Seeber, L., and A. Pêcher (1998), Strain partitioning along the Himalayan arc and the Nanga Parbat antiform, *Geology*, 26, 791–794, doi:10.1130/0091-7613(1998)026<0791:SPATHA>2.3.CO;2.
- Sharma, K. K., and K. R. Gupta (1978), Some observations on the geology of the Indus and Shyok valleys between Leh and Panamik, District of Ladakh, Jammu and Kashmir, India, *Recent Res. Geol.*, 7, 133–143.
- Smith, H. A. (1993), Characterization and timing of metamorphism within the Indo-Asian suture zone, Himalayas, northern Pakistan, Ph.D. thesis, Dartmouth Coll., Hanover, N. H.
- Smith, H. A., C. P. Chamberlain, and P. K. Zeitler (1992), Documentation of Neogene regional metamorphism in the Himalayas of Pakistan using U-Pb in monazite, *Earth Planet. Sci. Lett.*, 113, 93–105, doi:10.1016/0012-821X(92)90213-F.
- Steck, A. (2003), Geology of the NW Indian Himalaya, *Eclogae Geol. Helv.*, 96(2), 147–196.
- Tahirkheli, R. A. K. (1982), Geology of the Himalaya, Karakoram, and Hindu Kush in Pakistan, *Geol. Bull.*, 15, 51 pp., Univ. of Peshawar, Peshawar, Pakistan.
- Tahirkheli, R. A. K. (1996), Map of tectonostratigraphic domains of Northern Collisional belts in Pakistan, scale 1:750000, MinRock Found., Geosci. Lab., Geol. Surv. of Pakistan, Islamabad.
- Tahirkheli, R. A. K., M. Mattauer, F. Proust, and P. Tapponnier (1979), The India-Eurasia suture zone in northern Pakistan: Synthesis and interpretation of recent data of plate scale, in *Geodynamic of Pakistan*, edited by A. Farah and de K. A. S. Jong, pp. 125–130, Geol. Surv. of Pakistan, Quetta.
- Treloar, P. J., et al. (2000), Geochronological constraints on the evolution of the Nanga parbat syntaxis, Pakistan Himalaya, in *Tectonic of the Nanga Parbat Syntaxis and the Western Himalaya*, edited by M. A. Khan et al., *Geol. Soc. Spec. Publ.*, 170, 137–162.
- Valdiya, K. S. (1998), *Dynamic Himalaya*, 178 pp., Univ. Press, Hyderabad.
- Valli, F., N. Arnaud, P. H. Leloup, E. R. Sobel, G. Mahéo, R. Lacassin, S. Guillot, H. Li, P. Tapponnier, and Z. Xu (2007), Twenty million years of continuous deformation along the Karakoram fault, western Tibet: A thermochronological analysis, *Tectonics*, 26, TC4004, doi:10.1029/2005TC001913.
- Van Melle, J., P. A. van der Beek, S. Guillot, A. Pêcher, and M. Latif (2007), Slow steady exhumation of the high elevation Deosai Plateau (northern Pakistan Himalaya) since 40 Ma, *Eos Trans. AGU*, 88(52), Fall Meet. Suppl., Abstract T20-7345.
- Viganò, A., and S. Martin (2007), Thermorheological model for the European central Alps: Brittle-ductile transition and lithospheric strength, *Terra Nova*, 19, 309–316, doi:10.1111/j.1365-3121.2007.00751.x.
- Villa, I. M., Y. Lemennicier, and P. Le Fort (1996), Late Miocene to early Pliocene tectonometamorphism in south-central Karakoram and Indus-Tsangpo suture, Chogo Lungma area (NE Pakistan), *Tectonophysics*, 260, 201–214, doi:10.1016/0040-1951(96)00086-8.
- Wadia, D. N. (1975), *Geology of India*, 4th ed., 508 pp., Tata McGraw-Hill, New Delhi.
- Winslow, D. M., P. K. Zeitler, C. P. Chamberlain, and L. S. Hollister (1994), Direct evidence for a steep geotherm under conditions of rapid denudation, western Himalaya, Pakistan, *Geology*, 22, 1075–1078, doi:10.1130/0091-7613(1994)022<1075:DEFASG>2.3.CO;2.
- Yamaji, A. (2000), The multiple inverse method: A new technique to separate stresses from heterogeneous fault slip data, *J. Struct. Geol.*, 22, 441–452, doi:10.1016/S0191-8141(99)00163-7.
- Yamaji, A., S. Tomita, and M. Otsubo (2005), Bedding tilt test for paleostress analysis, *J. Struct. Geol.*, 27, 161–170, doi:10.1016/j.jsg.2004.08.006.
- Zanchi, A., and M. Gaetani (1994), Introduction to the geological map of the North Karakoram Terrain from the Chapursan valley to the Shimshal Pass 1:150000 scale, *Riv. Ital. Paleontol. Strat.*, 100, 125–136.
- Zanchi, A., and D. Gritti (1996), Multistage structural evolution of Northern Karakoram (Hunza region, Pakistan), *Tectonophysics*, 260, 145–165, doi:10.1016/0040-1951(96)00081-9.
- Zeitlinger, G., J.-P. Burg, N. Chaudhry, H. Dawood, and S. Hussain (2000), Fault systems and paleo-stress tensors in the Indus Suture Zone (NW Pakistan), *J. Asian Earth Sci.*, 18(5), 547–559, doi:10.1016/S1367-9120(99)00084-X.
- Zeitlinger, G., D. Seward, and J.-P. Burg (2007), Exhumation across the Indus suture zone: A record of back sliding of the hanging wall, *Terra Nova*, 19(6), 425–431, in press., doi:10.1111/j.1365-3121.2007.00767.x.
- Zeitler, P. K. (1985), Cooling history of the NW Himalaya, Pakistan, *Tectonics*, 4(1), 127–151, doi:10.1029/TC004i001p00127.
- Zeitler, P. K., C. P. Chamberlain, and H. A. Smith (1993), Synchronous anatexis, metamorphism, and rapid denudation at Nanga Parbat (Pakistan Himalaya), *Geology*, 21, 347–350, doi:10.1130/0091-7613(1993)021<0347:SAMARD>2.3.CO;2.
- Zeitler, P. K., et al. (2001a), Crustal reworking at Nanga Parbat, Pakistan: Metamorphic consequences of thermal-mechanical coupling facilitated by erosion, *Tectonics*, 20, 712–728, doi:10.1029/2000TC001243.
- Zeitler, P. K., et al. (2001b), Erosion, Himalayan geodynamics, and the geomorphology of metamorphism, *GSA Today*, 11, 4–9, doi:10.1130/1052-5173(2001)011<0004:EHGATG>2.0.CO;2.

S. Guillot, A. Pêcher, P. van der Beek, and J. Van Melle, LGCA, CNRS, Université de Grenoble, BP 53, F-38041, Grenoble, France. (arnaud.pecher@ujf-grenoble.fr)

F. Jouanne and J. L. Mugnier, Laboratoire de Géodynamique des Chaînes Alpines, CNRS, Université de Savoie, Campus Scientifique, F-73376, Le Bourget du Lac, France.

A. Kausar, M. Latif, and A. Majid, Geological Survey of Pakistan, Plot No. 84, H-8/1, Islamabad, Pakistan.

G. Mahéo, Laboratoire de Sciences de la Terre, CNRS, Université de Lyon 1 et ENS de Lyon, 2 rue R. Dubois, F-69622, Villeurbanne, France.

Y. Rolland, Géosciences Azur, UMR 6526, CNRS, Université de Nice, BP 2135, F-06103, Nice, France.

L. Seeber, Lamont-Doherty Earth Observatory, Earth Institute at Columbia University, Palisades, NY 10964, USA.